Journal of Materials Chemistry B

ROYAL SOCIETY OF CHEMISTRY

REVIEW

View Article Online
View Journal | View Issue

Cite this: J. Mater. Chem. B, 2024, 12, 1149

Optical imaging probes for selective detection of butyrylcholinesterase

Musa Dirak, [a] Jefferson Chan [b] and Safacan Kolemen *[a]

Butyrylcholinesterase (BChE), a member of the human serine hydrolase family, is an essential enzyme for cholinergic neurotransmission as it catalyzes the hydrolysis of acetylcholine. It also plays central roles in apoptosis, lipid metabolism, and xenobiotic detoxification. On the other side, abnormal levels of BChE are directly associated with the formation of pathogenic states such as neurodegenerative diseases, psychiatric and cardiovascular disorders, liver damage, diabetes, and cancer. Thus, selective and sensitive detection of BChE level in living organisms is highly crucial and is of great importance to further understand the roles of BChE in both physiological and pathological processes. However, it is a very complicated task due to the potential interference of acetylcholinesterase (AChE), the other human cholinesterase, as these two enzymes share a very similar substrate scope. To this end, optical imaging probes have attracted immense attention in recent years as they have modular structures, which can be tuned precisely to satisfy high selectivity toward BChE, and at the same time they offer real time and nondestructive imaging opportunities with a high spatial and temporal resolution. Here, we summarize BChE selective imaging probes by discussing the critical milestones achieved during the development process of these molecular sensors over the years. We put a special emphasis on design principles and biological applications of highly promising new generation activity-based probes. We also give a comprehensive outlook for the future of BChE-responsive probes and highlight the ongoing challenges. This collection marks the first review article on BChE-responsive imaging agents.

Received 19th October 2023,
Accepted 2nd January 2024

DOI: 10.1039/d3tb02468g

rsc.li/materials-b

Introduction

Butyrylcholinesterase (BChE; EC 3.1.1.8.) is an ~85 kDa α-glycoprotein that is a member of the serine hydrolase family.[1–5] Investigation of BChE, together with acetylcholinesterase (AChE; EC 3.1.1.7.), dates back to 1932.[6] AChE is mainly responsible for the hydrolysis of acetylcholine (ACh), while BChE hydrolyzes various choline conjugates including ACh, succinylcholine and butyrylcholine, in addition to a range

[a] Department of Chemistry, Koç University, 34450 Istanbul, Turkey. E-mail: skolemen@ku.edu.tr
[b] Department of Chemistry, Beckman Institute for Advanced Science and Technology, and Cancer Center at Illinois, University of Illinois at Urbana-Champaign, Urbana, Illinois 61801, USA

Safacan Kolemen and Musa Dirak

Musa Dirak obtained his BSc degree in Chemistry at Istanbul Technical University. Currently, he is pursuing his PhD studies under the supervision of Dr Safacan Kolemen at Koç University. His research interest focuses on the development of activity-based probes for tumor imaging and therapy. Dr Safacan Kolemen earned his PhD degree at Bilkent University in 2014. After working as a postdoctoral researcher at UC Berkeley, he joined Koç University as an Assistant Professor and started his independent research laboratory in 2017. His current research focuses on the development of tumor selective phototherapy agents and fluorescent/chemiluminescent molecular sensors for bioimaging applications.

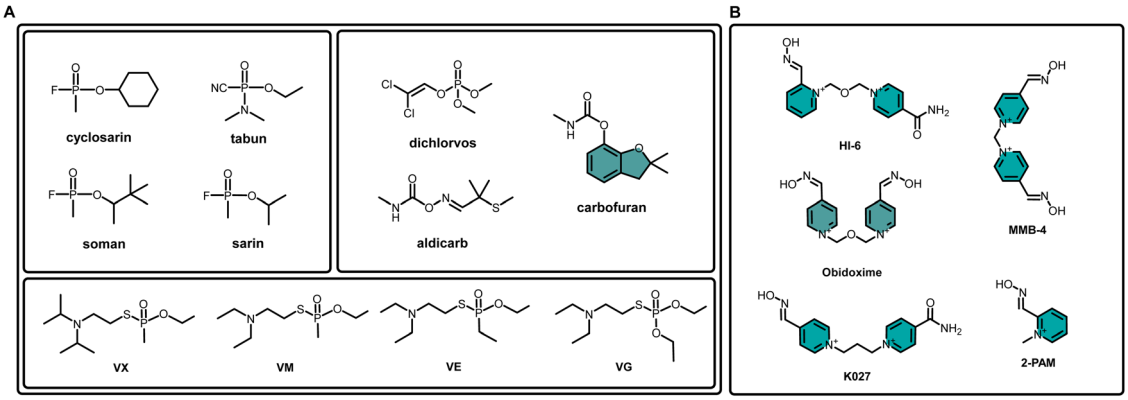

Fig. 1 (A) Molecular structures of nerve agents, selected OPs and (B) oxime derivatives.

of non-choline conjugates such as heroin, cocaine, and aspirin.[4,7–16] BChE has been referred to as acylcholine acylhydrolase, plasma cholinesterase, pseudocholinesterase, non-specific cholinesterase or serum cholinesterase in the previous reports.[1–3,17,18] However, the name "butyrylcholinesterase" was given to the enzyme by the Committee for Human Gene Nomenclature in 1989.[19]

Fluctuations of BChE is a good indicator for exposure of nerve agents, extremely poisonous organophosphates (OPs), as they are known to inhibit BChE activity.[20–23] Notably, OPs are not only used as pesticides in agriculture but also used as a biological weapon.[21,22,24–29] To this end, it became a threat to both national security and public health. BChE is inhibited as a result of the reaction taking place between the nerve agent and serine, which consequently deactivates the OPs.[21] One characteristic feature of this reaction is that OP adducts on BChE can be detected by mass spectrometry.[30–32] Additionally, BChE enzyme inhibited by OPs can be reactivated with numerous oximes.[20,21,33–35] Frequently encountered nerve agents including V-type (VX, VM, VE, VG), G-type (soman, sarin, tabun, cyclosarin), and neurotoxic pesticides including aldicarb, carbofuran, and dichlorvos were depicted in Fig. 1A.[22,28,32,36–39] Additionally, most common reactivators reported in the literature were summarized in Fig. 1B.

Jefferson Chan

Prof. Jeff Chan began his independent career in 2014 and was promoted to the rank of Associate Professor in 2021. His research interests include the development of activity-based sensing probes for biomedical applications, design of tools to study the chemical biology of aging and associated diseases, and the application of new chemistry for targeted drug delivery.

Understanding the role of BChE and its differentiation from AChE is vital, particularly in ACh hydrolysis. Customarily, BChE does not play a key role in ACh hydrolysis since its complete inhibition bears no impact on muscle contraction.[21,40] Indirect evidence collected from knockout mice studies suggest that inhibition of AChE with huperzine A or donepezil in BChE deficient animals results in fatality as opposed to AChE knockout mice with normal levels of BChE. Accordingly, no toxicity is observed in mice with normal levels of AChE and BChE, concluding hydrolysis of ACh by BChE since the cause of death is reported as tonic convulsions, a symptom indicating ACh abundance.[41] Additionally, introducing a nerve agent VX into an AChE knockout mouse develops symptoms of cholinergic toxicity, which is attributed to the excess ACh as a result of BChE inhibition.[42] Those results lead us to a point where BChE acts as a back-up enzyme in the absence of AChE. One may conclude that elevated levels of BChE in human plasma is beneficial in case of fluctuations of AChE or exposure of OPs. Despite its potential, the absence of BChE in humans exhibits no adverse effects under normal conditions.[43] However, its plausible effect on OP exposure has been validated in animal models with the utilization of BChE purified from human serum or equine, and the safety of introducing BChE in human subjects has been demonstrated.[44–49] One limitation to its clinical application is the expensive and difficult purification steps as resources for the production are limited.[50,51] Another setback is keeping the enzyme for a long time in the circulation.[51] Moreover, it is a stoichiometric reaction where only one molecule of BChE inhibits one molecule of OP, leading to the inactivation of BChE.[21] Just recently, a new method was developed for the purification of BChE from frozen Cohn fraction IV-4 with higher yields (46%) compared to other conventional methods (21%).[52] Also, a new nano capsule system offering a higher circulation half-time was developed by Jiang *et al.*, in 2016.[51] Overall, it is apparent that BChE has the potential to inhibit OPs, and recent findings support its utilization. Although BChE has been employed in numerous incidents, it requires further optimization and investigation before it paves the way for clinical translation.[24,51]

Intensive research has been carried out on purification of BChE over the years and procedures have been well-estab-

lished. BChE can be purified from outdated human plasma or Cohn Fraction IV-4. In general, two subsequent purification steps are followed for purification of BChE: (1) anion exchange is performed at pH 4 or pH 4.5, and (2) affinity chromatography is employed by using columns packed with Procainamide-Sepharose affinity medium.[53] In 2012, huprine affinity gel was proposed to be superior due to its higher binding capacity and specificity for BChE compared to procainamide.[24,54,55] Accordingly, the purification of BChE on huprine-Sephraose results in a purity level of 54–90%, while it is only 3–8% for procainamide-Sephrose.[24,56] The mentioned strategies are well defined and employed in numerous studies; however, a cost-effective protocol was developed by Mehrani, in 2003.[57] In this work, BChE was purified from human plasma using polyethylene glycol precipitation and ion exchange chromatography with ~30% purity. BChE can also be purified from human plasma using monoclonal antibodies.[58–62] Currently, high purity (99%) BChE can be produced with a yield of 22% using common methods, but an optimized procedure has been reported to have a 46% yield with the same purity level (99%) as the ion exchange step was eliminated.[52]

Stability of the enzyme is as important as the purification and isolation processes. Stability of BChE in human plasma or after purification were assessed at different temperatures in various studies. Less than 10% of BChE activity was lost when human plasma was stored for 50 days at 4 °C or −20 °C.[63] Superior to that, BChE purified from human plasma retained its activity for 2 years in lyophilized form at 4, 25, 37, 45 and −20 °C.[64] Similarly, BChE was also stable for 2 years when it was stored at 4 or 25 °C in its liquid form.[65] However, BChE has remained stable for at least 20 years at 4 °C, when stored under sterile conditions.[24] In general, it is very likely to lose activity in dilute solution for enzymes when the concentration is less than 1 mg mL^{-1}.[66] One route to prevent degradation and activity loss is addition of albumin (1–5 mg mL^{-1}).[66,67] At low temperatures, formation of ice crystals damages the protein structure.[66,68,69] In that case, cryoprotectants such as glycerol or ethylene glycol can be selected as stabilizers.[66] However, the binding effect varies, and it is specific to the protein of interest. Additionally, it requires further investigation for each enzyme individually due to its unique effect on their hydrophobic or hydrophilic interactions at different concentrations or pH values.[70–72] Therefore, a stabilizer must be chosen accordingly. For instance, while glycerol is suitable for BChE, it may not suitable for other enzymes.[70] Accordingly, BChE solution less than 1 mg mL^{-1} might lose its activity completely when frozen and thawed. Therefore, dilute solutions of BChE suggested to be kept in 20% glycerol. Despite this, dilute solutions of BChE retains its activity in Tris-buffer, as opposed to AChE, which requires albumin (1 mg mL^{-1}) for stabilization. However, in the concentration range of 1 to 10 mg mL^{-1}, no loss in activity was observed when the solutions were frozen and thawed, even in the absence of glycerol or albumin.[24]

BChE is widely distributed in the body but it is mostly found in the plasma and liver.[12,43] However, it is also expressed in skin, leg muscle, small intestine, lungs, cerebral cortex, stomach, spleen, kidney, cerebellum, heart, medulla oblongata, and thyroid.[43] As BChE is found to be most abundant in plasma, its average concentration was investigated in different studies, revealing varying concentrations of BChE in human plasma between 3.5 and 9.3 mg L^{-1}.[24,73–76] Additionally, the structure of BChE has been investigated extensively and the catalytic triad of BChE was identified as Ser 198, His 438, and Glu 325.[77,78] It is highly critical to identify the structural differences between AChE and BChE to understand their discriminatory behavior toward ligands with different sizes. To that end, the main, side, back and acyl loop doors of AChE and BChE were investigated using molecular dynamic simulations on their monomer and tetramer structures, and the structural differences between AChE and BChE were marked in detail. The maximum radii of the main door, side door, back door and acyl loop door for AChE monomer was reported as 2.30 Å, 2.10 Å, 1.80 Å and 1.50 Å, while it was found to be 4.00 Å, 2.30 Å, 2.30 Å and 1.70 Å for BChE monomer, respectively. Similarly, 4 subunits at the catalytic domain were also analyzed. The maximum radii of the main door for AChE tetramer were 2.40 Å, 1.30 Å, 2.30 Å and <1.20 Å, while they were 3.70 Å, 2.60 Å, 3.40 Å, and 2.80 Å for the BChE tetramer.[79] It is evident that BChE holds a larger door radius than AChE, which provides compelling evidence of why larger ligands can be hydrolyzed by BChE, as opposed to AChE, which is specific to small substrates such as ACh.

Additionally, the structural differences between AChE and BChE were also evaluated by comparing the aromatic residues laying around the main entrance. The three aromatic residues (Tyr 341, Trp 286, and Tyr 72) were associated with the entrance of active site, and the other five (Phe 338, Tyr 337, Phe 297, Phe 295, and Tyr 124) were located at the equal depth within the gorge. In the BChE structure, the residues, Tyr 72, Tyr 124, Trp 286, Phe 295, Phe 297 and Tyr 337 were replaced with Asn 68, Gln 119, Ala 277, Leu 286, Val 288, and Ala 328, respectively (Fig. 3). This allows the hydrolysis of larger substrates as the replaced residues are smaller than those located in AChE.[79]

Initially, the physiological role of BChE was misinterpreted as a 52 year old female patient with silent BChE was observed to have no detectable impairment in health.[80] Yet, it has been confirmed that hydrolysis of succinylcholine was hampered due to silent BChE. Moreover, it is evident that BChE is involved in numerous physiological processes and diseases including fat metabolism, detoxification, insulin resistance, Alzheimer's and Parkinson's diseases, liver damage, cardiovascular disorders, inflammation, anorexia nervosa, HELLP syndrome, depression and cancer (Fig. 2).[81–93] Accordingly, the monitoring of BChE becomes a highly important task due to potential involvement of BChE in physiological and pathological processes, as well as its association with various conditions.

The latest findings indicated that the level of BChE was significantly elevated in Alzheimer's Disease (AD).[94] Although a couple of reports indicate the BChE levels in AD as the same, BChE still holds the potential to be a biomarker for AD.[95] In contrast to BChE, the levels of AChE have been shown to decrease in AD.[94,95] Ghrelin is a 28-amino acid peptide and an orexigenic hormone, which is known to stimulate appetite, as

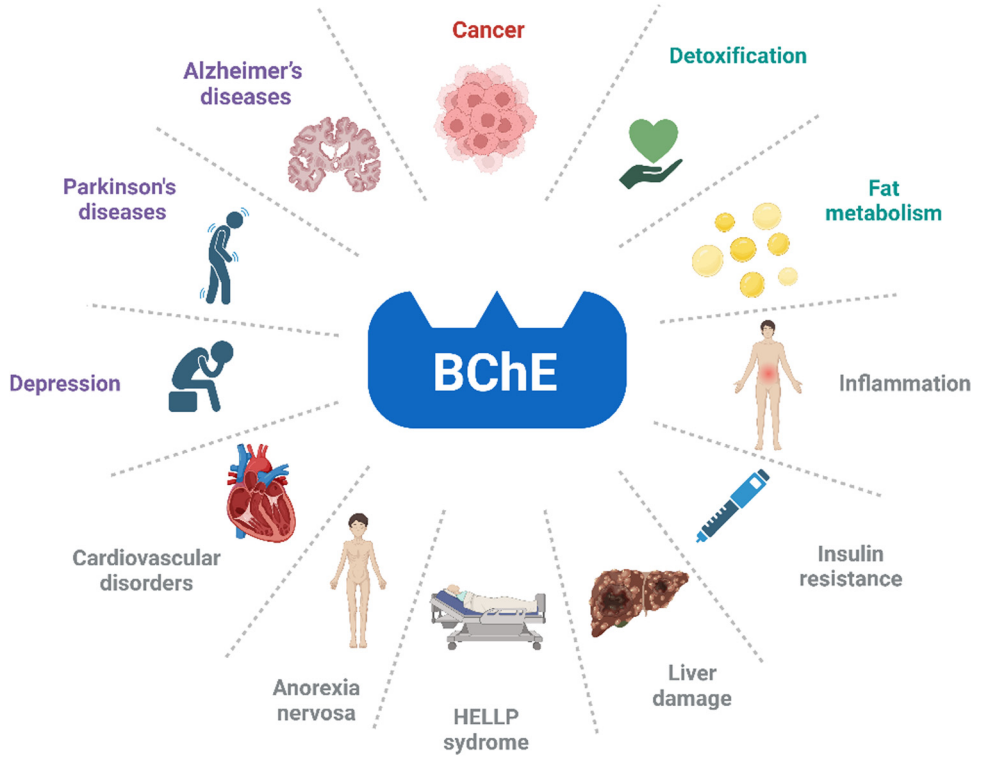

Fig. 2 BChE associated diseases and conditions.

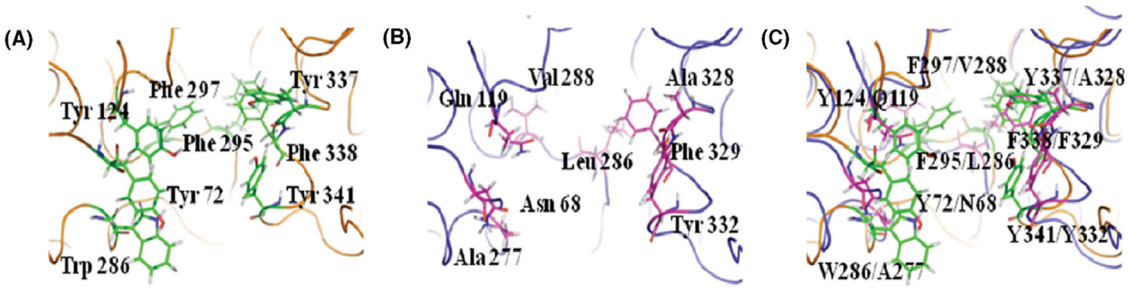

Fig. 3 The residues in the gorge of (A) AChE, (B) BChE, and (C) superimposing of the gating residues in AChE and BChE. Adapted with permission from ref. 79. Copyright 2011 American Chemical Society.

its concentration increases during fasting but decreases after consuming food. The hydrolysis of ghrelin to desacyl ghrelin by BChE gives its inactive form, affecting weight gain and glucose homeostasis.[43,96–99] For instance, BChE knockout studies on mouse models showed that a high fat diet on mice resulted in obesity.[100] While this weight gain was attributed to the involvement of BChE in fat utilization, the hydrolysis of ghrelin by BChE is extraordinary since ghrelin is a large substrate with a molecular weight of 3369 Da, making ghrelin the largest substrate for BChE.[100,101] This unusual hydrolysis has raised a question of whether BChE is the responsible enzyme for the ghrelin hydrolysis. Consequently, five batches of human BChE with over 98% purity were prepared, and all of them hydrolyzed ghrelin to desacyl ghrelin, which was also supported through inhibition studies.[101] Additionally, molecular docking studies revealed the distance between the serine oxygen and carbonyl carbon of octanoyl as 4.2 Å, which was shorter than the distance recorded during cocaine-BChE simulations.[102]

The most common method for the determination of BChE activity is the well-known Ellman's method which is based on the hydrolysis of butyrylthiocholine to give thiocholine. Consecutively, the resultant thiol cleaves the disulfide bond of 5,5′-dithiobis-2-nitrobenzoic acid (DTNB), also known as Ellman's reagent, to give TNB, a yellow substrate, and its absorbance at 412 nm is an indicator of the BChE activity (Fig. 4).[103] Ellman's method can also be applied for the determination of AChE activity using acetylthiocholine (Fig. 4). Therefore, it became a standard method for the determination of cholinesterase activity; however, it suffers from low sensitivity, and selectivity due to the fact that different matrixes including sulfhydryl groups, inhibitors and oximes might cause a direct or indirect interference, affecting the reliability of the Ellman's method.[20,103–105]

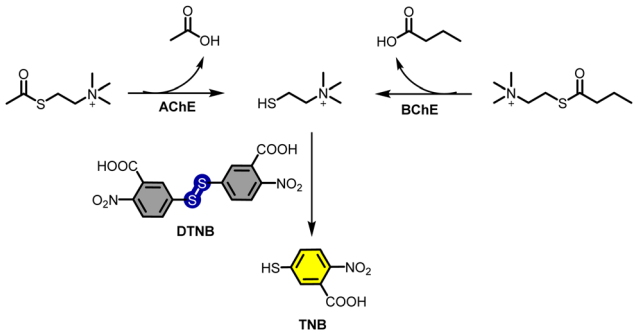

Fig. 4 Schematic illustration of Ellman's method.

BChE can also be detected through enzyme-linked immunosorbent assay (ELISA) and electrochemical methods.[106,107]

Fluorescence imaging has attracted great attention in recent years due to its capability for real-time monitoring of targeted analytes with a high selectivity and sensitivity.[108] Fluorescent probes are designed in a way to give a signal upon binding or after reacting with a targeted analyte as their photophysical properties are altered. In general, the radiative pathways of the fluorescent probes are activated or quenched through intermolecular charge transfer (ICT), photoinduced electron transfer (PET), Förster resonance energy transfer (FRET) and aggregation induced emission (AIE) mechanisms.[109] Most encountered analytes for binding type fluorescent probes are ions and charged species while activity-based sensing utilizes enzymes, reactive oxygen species, biothiols and reactive nitrogen species.

It is much more challenging to establish a masking unit for enzymes compared to other analytes as identification of a recognition moiety with high selectivity and sensitivity is difficult. One way to design a specific substrate is by mimicking inhibitors of the targeted enzymes. To that end, repeating functional groups of inhibitors are typically constructed on a self-immolative linker to determine fluorescence signal upon cleavage. One benefit of this approach is the ease of assessing the sensitivity towards the targeted enzyme. Another advantage is the modularity of the masking units, which allows to find the best structure fitting the enzyme pocket by simple synthetic modifications. For instance, the dimethyl carbamate moiety can be hydrolyzed by AChE, BChE and CE. However, the modification at the *ortho* position of dimethyl carbamate unit with different functional groups results in variations in the response of the masking unit.[110] In addition to that, pK_a of the resulting phenol after the cage removal can be lowered to give stronger signal at physiological pH by substituting *ortho* or *para* position with electron withdrawing groups. In accordance with esterases, identification of a masking unit with a fast response time and high selectivity is also applicable for other enzymes, such as monoamine oxidase A/B and alpha-L-fucosidase (AFU), when this approach was employed.[111,112]

BChE has been studied extensively over the past decades, and mostly, its activity has been measured indirectly through Ellman's method. However, introduction of BChE-responsive moiety opened a new gateway for real-time monitoring of BChE activity, and numerous molecular sensors were employed for direct investigation of its relation between different disease states and conditions. Several studies have already reported the recent progress on detecting CE activity,[113–116] and just recently, AChE-responsive fluorescent probes were summarized in a review paper.[117] This review reports the recent progress on BChE-responsive imaging probes and their bio-applications with a special emphasis on design principles. To our knowledge, this is the first review article covering BChE selective molecular sensors. We also provide our insight and outlook on the field while discussing the future directions.

BChE responsive molecular sensors

Two fluorescent probes (**1a** and **1b**) with similar structures were developed by Chao *et al.*, in 2016 (Fig. 5).[118] The probes were synthesized by a coupling reaction between commercially available Cyanine 5.0 dye and Huprine, a potent AChE and BChE inhibitor. However, **1a** and **1b** were determined to be 1250- and 403-fold more sensitive to AChE than BChE, respectively. Also, the probes were always in a fluorescence-on mode which is not favored in fluorescence imaging as fluctuations cannot be monitored.

In 2016, Han's group constructed a BChE-responsive fluorescent probe (**2**) based on a 4,5-dimethoxyphthalimide scaffold that was extended with a choline conjugate (Fig. 6).[119] The probe was initially in its on-state; however, hydrolysis of the choline-based ester by BChE resulted in quenching of the

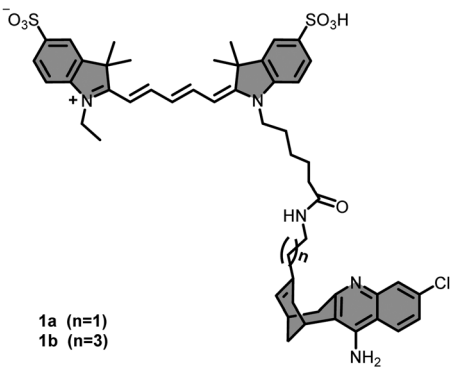

Fig. 5 Molecular structures of compound **1a** and **1b**.

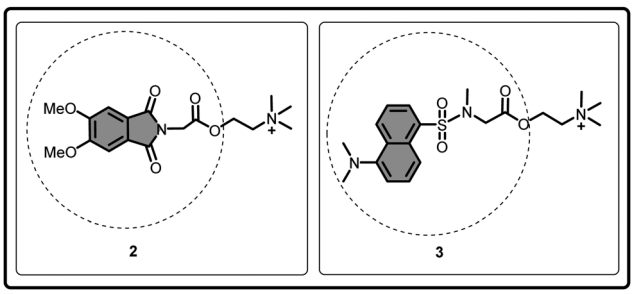

Fig. 6 Molecular structure of compound **2** and **3**.

fluorescence at 520 nm upon excitation at 355 nm due to the PET modulation at neutral pH. The probe exhibited a linear turn-off response to BChE in the concentration regime of 1–10 U mL^{-1} but the fluorescence signal of the probe remained almost identical even in the presence of high concentration (150 U mL^{-1}) of AChE, confirming its selectivity. The probe was also employed successfully for assessing inhibition efficiency of two BChE inhibitors, tacrine and galantamine. However, turn-off fluorescent sensors are not ideal for complex applications as their fluorescence can be quenched through BChE-independent mechanisms in the cellular environment.

Dansyl-L-sarcosine (DS), a fluorophore specifically known with its enhanced fluorescence emission after binding to human serum albumin, was caged with an ACh to obtain BChE-responsive fluorescent probe (**3**) by the same group (Fig. 6).[120] The probe **3** bears a dual locked system as it requires consecutive activation by BChE and HSA before enhancing its emission. The probe **3** exhibited no significant response to BChE or HSA alone; however, its fluorescence at 485 nm, upon irradiation at 340 nm, was notably enhanced in the co-presence of BChE and HSA. Moreover, in the presence of HSA (20 μM), the probe **3** displayed a linear response (R^2 = 0.99746) to BChE concentration within the 0–2 U mL^{-1} range, and its LOD was calculated as 0.0012 U mL^{-1}. Favorably, probe **3** displayed no response to AChE, even at high concentrations (20 U mL^{-1}). The probe was utilized to determine the BChE content in human serum without HSA, as the serum itself contains sufficient HSA to increase the emission upon hydrolysis of ACh by BChE. BChE activity was measured as 5.723 ± 0.0014 U mL^{-1}. In support of this result, Ellman's method measured a similar BChE activity, which was reported as 5.720 ± 0.0085 U mL^{-1}.

In 2017, pioneering work by Yang's group introduced the first example of a highly selective BChE responsive masking unit.[121] Initially, several fluorescent cores, including cyanine, hemicyanine, coumarin, naphthalimide, and fluorescein skeletons (Fig. 7), were masked with a butyryl chain (**4–8**) to determine the most suitable fluorophore for detection of BChE. As a reference, an acetylthiocholine unit was selected. Among them, the masked methoxyfluorescein scaffold (**8**) displayed a 250-fold increase in the fluorescence channel, indicating its eligibility for BChE detection. After that, the methoxyfluorescein scaffold (**9**) was diversified with different alkyl chains and cycloalkyl substituents (**9a–9j**) to determine the ideal recognition moiety for BChE (Fig. 7). The cyclopropyl group (**9d**), surpassed the other substituents and exhibited a 14.5-fold selectivity for BChE over AChE. In the presence of BChE, the probe exhibited a 275-fold enhancement in the fluorescence signal at 515 nm upon excitation at 455 nm. Its selectivity toward BChE over AChE was supported by docking studies as a closer proximity of Ser-198 to the carbonyl moiety in the BChE active site (4.3 Å) was found in comparison to the AChE active site (7.4 Å). Probe **9d** was further used for monitoring the tacrine inhibition in the concentration region of 0.1–20 μM. The probe successfully monitored the endogenous BChE activity in living PANC-1 cells *via* confocal microscopy, both in the presence and absence of tacrine. One interesting aspect of this study is that it reported a very sensitive unit for BChE, which opens a gateway for the imaging of BChE activity. However, the study also investigated many other masking groups that are not as sensitive, thereby orienting future studies.

In 2018, the same group further developed a set of NIR-emitting BChE-responsive fluorescent probes by incorporating the BChE-sensitive cyclopropyl group into a series of well-known fluorescent scaffolds (Fig. 8) such as resorufin (**10**), DDAO (**11**), and hemicyanine (**12**).[122] Among them, probe **12**, the one with hemicyanine scaffold, exhibited lowest response to AChE while emitting the longest wavelength at 705 nm. **12** displayed superior selectivity (30.6-fold) for BChE over AChE compared to **9d**. After its photophysical characterization, compound **12** was employed for the detection of endogenous BChE activity in SH-SY5Y neuroblastoma cells. The red fluorescence of **12** (10 μM) was restored after hydrolysis by endogenous BChE. The emission signal was significantly reduced when SH-SY5Y cells were pretreated with tacrine and iso-OMPA, a BChE specific inhibitor. However, the emission signal recorded from SH-SY5Y cells were almost identical with the probe only group when the cells were pretreated with donepezil, an AChE specific inhibitor, concluding selective activation by endogenous BChE. This selectivity was also confirmed by utilizing compound **12** in

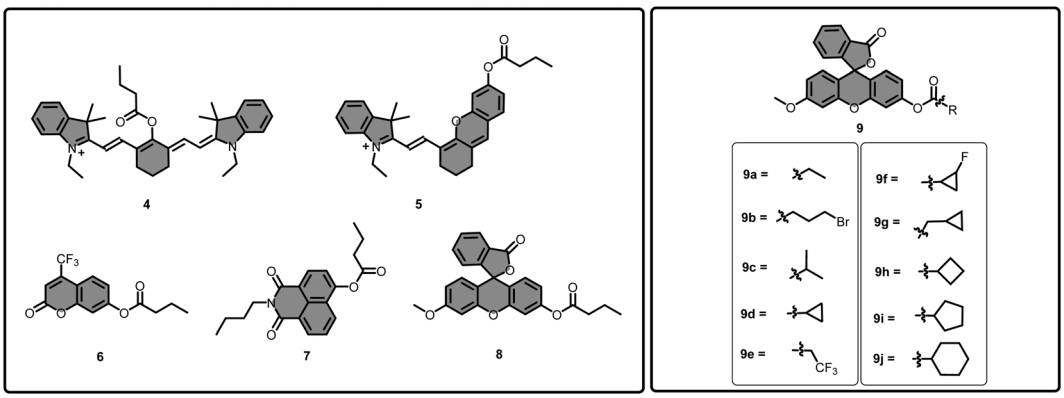

Fig. 7 Molecular structures of compound **4–9** and **9a–j**.

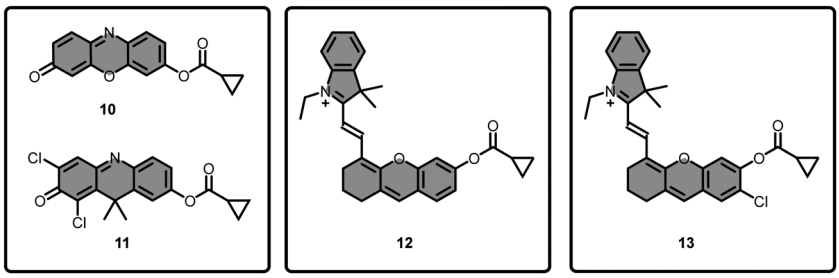

Fig. 8 Molecular structures of compound **10–13**.

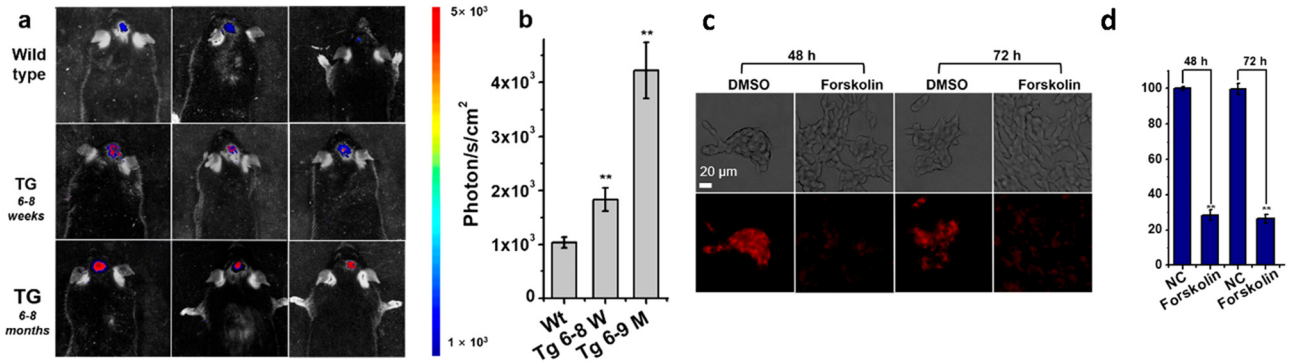

Fig. 9 (a) Confocal images of wild type, TG (6–8 weeks), and TG (6–8 months) mice after treatment with probe **12**. (b) Quantitative analysis of corresponding signals shown in (a). λ_{ex} = 650 nm, λ_{em} = 690–800 nm. (c) Confocal images of SH-SY5Y cells pre-incubated with 0.5% DMSO or forskolin for 48 or 72 h and then treated with probe **12**. (d) Relative emission intensities of the cells shown in (c). Adapted with permission under a Creative Commons CC BY License from ref. 122. Copyright 2018 American Chemical Society.

recombinant human BChE-expressing HEK293 cells and BChE knockdown SH-SY5Y cells. The probe successfully detected the reduced levels of BChE in SH-SY5Y cells treated with forskolin (Fig. 9), and additionally monitored selective BChE activation in zebrafish models using tacrine and donepezil inhibitors. **12** was also utilized to image transgenic mouse models bearing Alzheimer's disease (AD). The highest signal was acquired from older transgenic (TG) mice (6–9 months) relative to the young TG mice (6–8 weeks) and wild type (WT) mice groups, with the lowest signal recorded from the WT mice group (Fig. 9). Additionally, the probe successfully detected the elevated levels of BChE content in SHSY-5Y cells treated with $A\beta_{1-42}$ fibrils. Finally, impact of insulin resistance on BChE levels were evaluated as it was reported to be associated with AD. For that purpose, SH-SY5Y cells were treated with hydrocortisone to induce insulin resistance. Compound **12** displayed higher fluorescence signals than the non-treated groups, concluding raised levels of BChE. The authors highlighted two probable explanations: insulin resistance contributes to the BChE levels, or the enzyme is associated as a bridge between AD and type II diabetes. Overall, Yang's group initially developed a BChE sensing moiety, and further incorporated their masking group into a NIR-emitting fluorophore to investigate the BChE activity in complicated systems.

The literature indicates that the active site of AChE was located at the bottom of a deep 20-Å gorge and bearing a smaller cavity than BChE.[79] Followingly, Ma *et al.* acknowledged the work of Yang's group and further improved the selectivity of their NIR-emitting hemicyanine based probe (**12**) by chlorinating the phenolic hydroxyl of the fluorophore (Fig. 8) at the *ortho*-position in order to minimize the interference from AChE.[123] The chlorinated probe (**13**) responded to AChE with a fluorescence signal that was approximately four times weaker than as of **12**, demonstrating its increased selectivity. Addition of BChE into solution of **13** resulted in a red shift in the absorbance channel from 581 nm to 687 nm while activating its fluorescence at 708 nm. The LOD of the probe was calculated as 3.75 U L^{-1}. Molecular docking studies based on chemscore also supported its "anti-AChE" interference property due to the introduction of a bulky atom. The selective activation of **13** by endogenous BChE was demonstrated in HepG2 (Fig. 10) and LO2 cells. Inhibition of BChE by neostigmine bromide or tacrine significantly reduced the fluorescence in both cells; however, no inhibition was observed when the cells were pretreated with donepezil, an AChE specific inhibitor.

A novel redox-controlled nano-switch system (**14**) utilizing thiol-functionalized carbon quantum dots (CQD) for the detection of BChE was developed by Qian's group in 2018.[124] Disulfide-linkage between quantum dots can be cleaved by thiols to give fluorescence ON thiol-CQD. The fluorescence can be switched back to its OFF state by H_2O_2 (Fig. 11). By leveraging this property, butyrylthiocholine can be used as a thiol source, as its hydrolysis by BChE releases thiocholine, which is necessary to turn the fluorescence of the CQDs to its ON state. For more

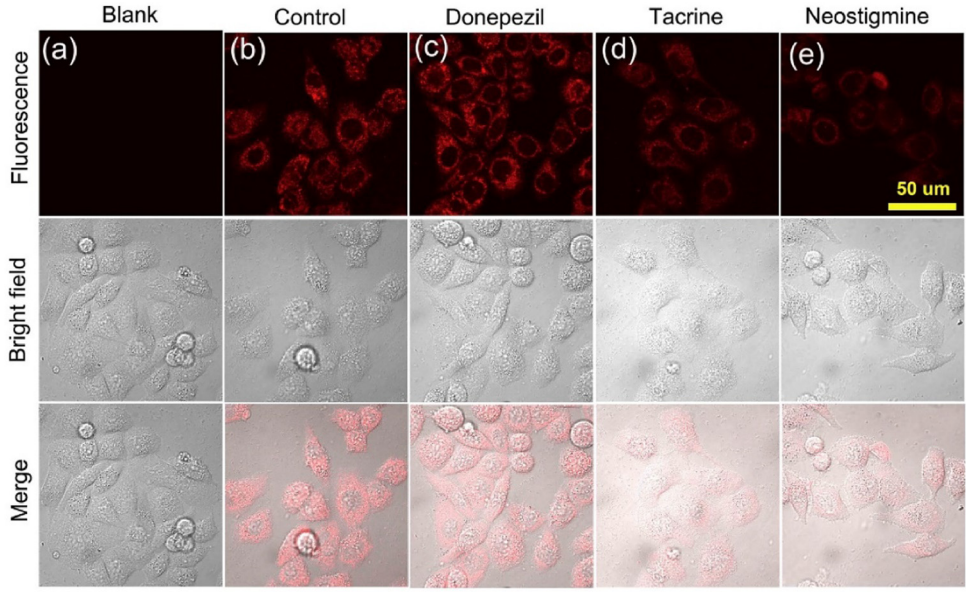

Fig. 10 (a) Confocal images of HepG2 cells in the absence of inhibitors and probe **13**. Confocal images of HepG2 cells (b) pre-incubated with donepezil (c), tacrine (d) or neostigmine (e) and then incubated with probe **13**. Adapted with permission from ref. 123. Copyright 2020 Elsevier.

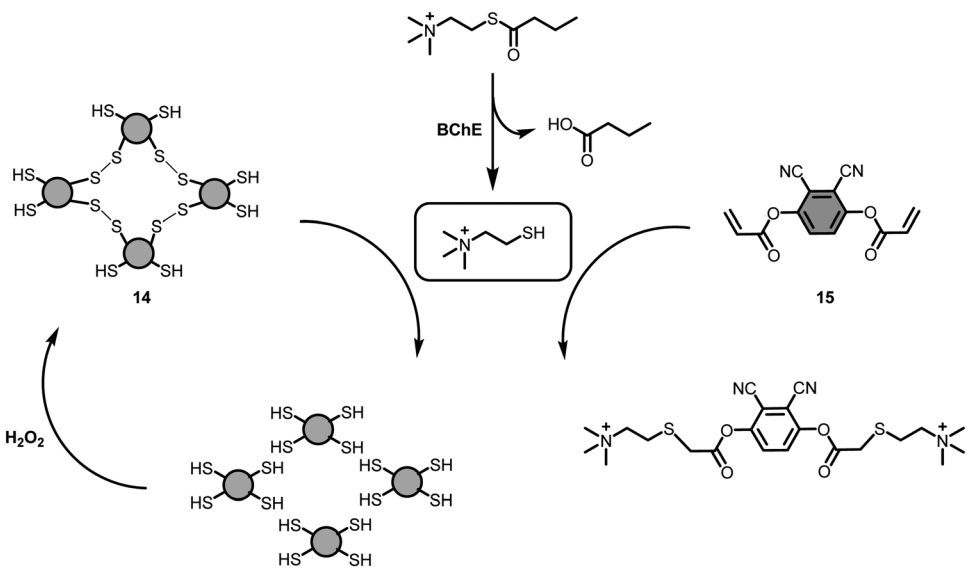

Fig. 11 Molecular structures and activation of compound **14** and **15** with BChE.

accurate detection of BChE activity, the impact of GSH and AChE were evaluated. In accordance with the theory, the emission of the thiol-CQDs around 523 nm switched to its ON and OFF state after consecutive addition of $Na_2S_2O_4$ (100 μM) and H_2O_2 (300 μM), respectively. The thiol-CQD (0.17 mg mL^{-1}) measured the BChE activity with high sensitivity (R^2 = 0.99) and LOD (2.7 U L^{-1}) in the concentration range of 60.0–220.0 U L^{-1}. Notably, the probe determined the BChE level in serum samples collected from three healthy male volunteers, and almost similar results were obtained when BChE levels were measured by Ellman's method, indicating its accuracy. Both results were in the range of the reported BChE levels for healthy individuals. This redox-controlled system can also evaluate the AChE activity as thiol source can be replaced, bearing a similar resemblance to Ellman's method.

In 2018, the same group introduced a butyrylthiocholine based, and thiol–ene click reaction driven fluorescent probe (**15**) for BChE detection (Fig. 11).[125] Initially, compound **15** displayed a weak fluorescence; however, its emission around 460 nm was considerably enhanced, due to altered radiative rate constant, with two consecutive reactions: hydrolysis of S-butyrylthiocholine iodide into butyrylthiocholine followed by a rapid thiol–ene reaction between **15** and previously released butyrylthiocholine. The fluorescence emission of **15** showed high linearity with concentration of BChE from 0.2 to

9.0 U L^{-1} and the limit of detection (LOD) of the method was calculated as 0.06 U L^{-1}. The possible interference from AChE and GSH were evaluated. The assay remained unaffected by AChE, however the presence of GSH caused varying impacts on the emission signal. This interference can be avoided with a slight change in the experimental procedure by addition of GSH prior to the introduction of butyrylthiocholine.

A carbon dot based ratiometric fluorescence probe (**16**), discriminating BChE and AChE from each other, was devised by Xu *et al.*, in 2019.[126] Monodispersed carbon dots with an emission wavelength of 460 nm were prepared from glycerol and (3-aminopropyl)triethoxysilane (APTES) using hydrothermal method. Fluorescence of the CDs at 460 nm was quenched by 2,3-diaminophenazine (oxOPD), which was generated through *in situ* oxidation of *o*-phenylenediamine (OPD) by Cu^{2+}, yielding a new emission peak at 570 nm. As specified earlier, acetylthiocholine or butyrylthiocholine can be hydrolyzed by AChE or BChE into thiocholine, respectively. Following the hydrolysis, the oxidation of OPD was prohibited as Cu^{2+} ions were captured by sulfhydryl groups. Consequently, the emission peak at 570 nm decreased, while a new emission peak at 460 nm emerged, reporting the enzyme activity. The method evaluated the AChE and BChE activity with high linearity ($R^2 \geq 0.99$) in the concentration range of 0.2–4.0 U L^{-1} and 0.1–1.2 U L^{-1}, and the LOD for AChE and BChE was calculated as 0.1 U L^{-1} and 0.04 U L^{-1}, respectively. The method successfully measured the AChE and BChE content in human whole blood.

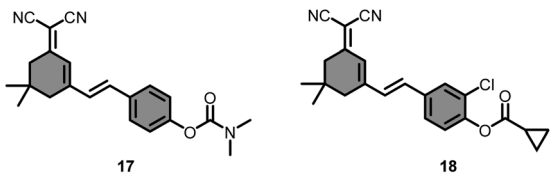

Fig. 12 Molecular structures of compound **17** and **18**.

A NIR-emitting fluorescent probe (**17**) for the detection of AChE and BChE (Fig. 12) was developed by Ma *et al.*, in 2020.[127] The probe was initially displaying a weak fluorescence as ICT was blocked; however, its fluorescence at 654 nm was recovered upon addition of AChE or BChE due to the hydrolysis of dimethyl carbamate moiety. The probe exhibited a high linear response (R^2 = 0.99) to AChE and BChE in the concentration region of 0–80 U mL^{-1} and 25–31 U mL^{-1}, respectively. The LOD for AChE and BChE was calculated as 0.127 U mL^{-1} and 0.0117 U mL^{-1}. Compound **17** successfully applied to monitor the cholinesterase activity in zebrafish, normal brain, and glioma.

Most of the dyes featuring small Stokes shifts often result in a low signal-to-noise ratio. The cyclopropyl moiety was incorporated into a chloro-substituted dicyanoisophorone skeleton (Fig. 12) to obtain an ICT-driven BChE sensitive probe (**18**).[128] The probe featured a large Stokes shift (110 nm) upon hydrolysis by BChE. Similar to other cyclopropyl bearing probes, compound **18** showed a linear (R^2 = 0.9995) turn-on response to BChE in the concentration range of 0–1.875 U mL^{-1} with a LOD of 0.08 U mL^{-1}. The probe turned to its ON state in HepG2 cells due to endogenous expression of BChE. Introduction of tacrine inhibited the BChE activity in HepG2 cells, and accordingly, its fluorescence was weakened. The probe further monitored the BChE activity in HepG2 tumor-bearing mice without leaking from the tumor site (Fig. 13).

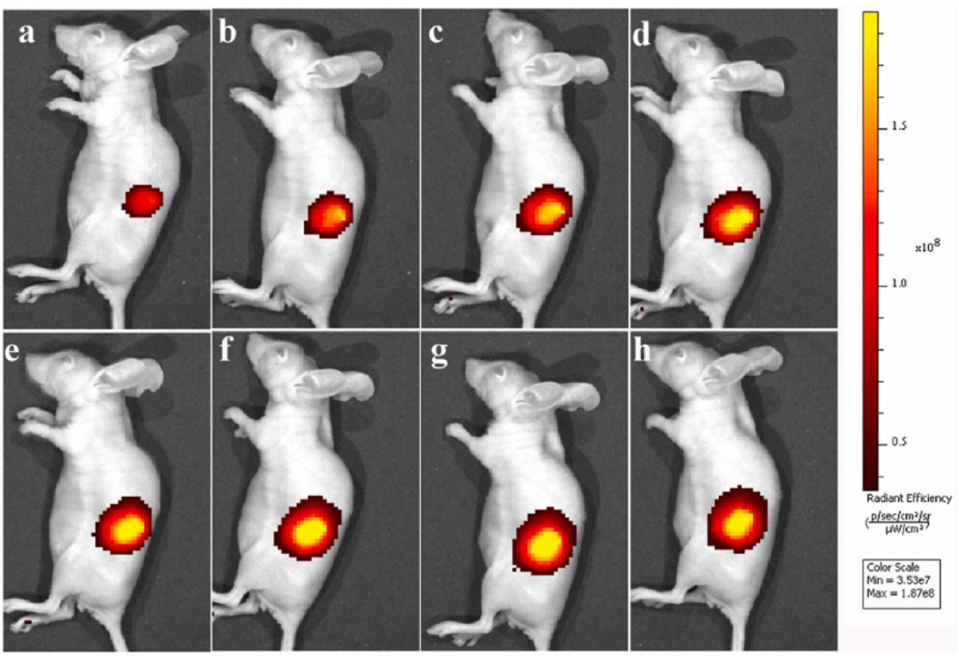

Fig. 13 Fluorescence images of HepG2-tumor bearing mice after intratumoral injection of probe **18**. Images were captured at different times point (a–h: 2, 5, 10, 15, 20, 25, 30, and 40 min). λ_{ex} = 500 nm, λ_{em} = 650–750 nm. Adapted with permission from ref. 128. Copyright 2022 Elsevier.

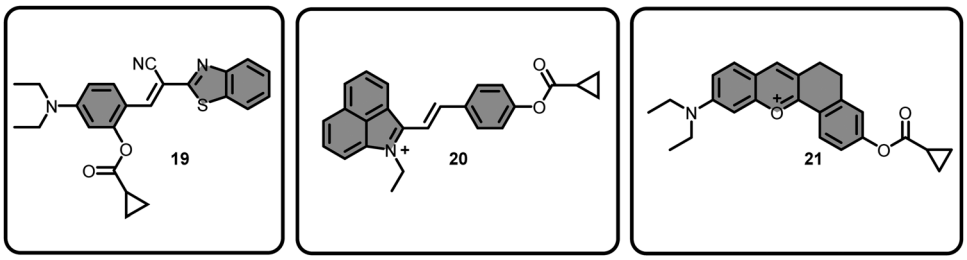

Fig. 14 Molecular structures of compound **19–21**.

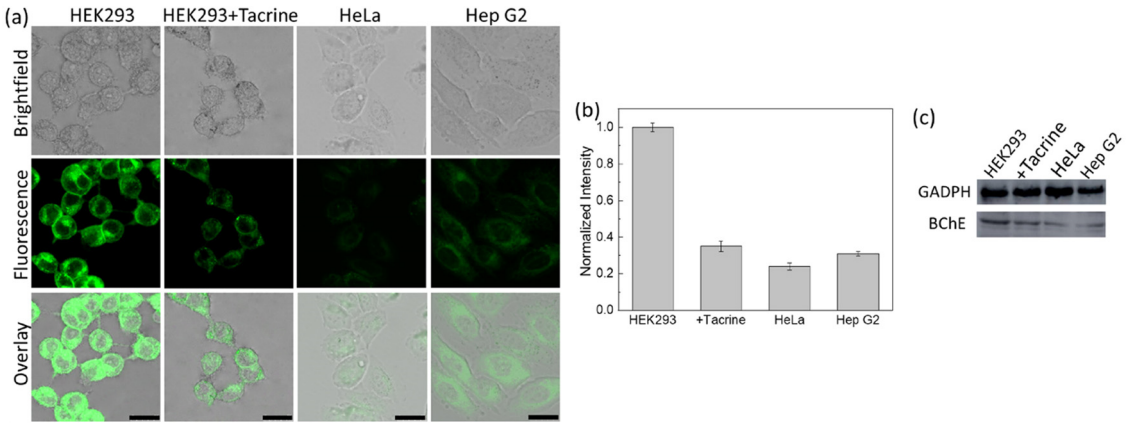

Fig. 15 (a) Confocal images of HEK293, HeLa and Hep G2 cells treated with probe **19**. Second row: HEK293 cells were pre-treated with tacrine and then incubated with probe **19**. (b) Normalized intensities of the cells shown in (a). (c) Expression of BChE activity monitored by western blot analysis in HEK293, HEK293 cells pretreated with tacrine, HeLa and Hep G2 cells. λ_{ex} = 458 nm. Adapted with permission from ref. 129. Copyright 2021 American Chemical Society.

A cyclopropyl moiety bearing BChE-responsive probe (**19**) was reported by Ding's group, in 2021 (Fig. 14).[129] No substantial alterations were detected in the absorption spectrum of **19** after BChE treatment; however, a significant but a linear (R^2 = 0.9939) turn-on response was monitored in the presence of BChE (0–7.0 μg mL^{-1}) with a LOD of 0.075 μg mL^{-1}. The probe displayed no response to AChE and CE in addition to elastase, tyrosinase and GSH, and monitored the endogenous BChE activity in HEK293, HeLa and HepG2 cells with respect to their BChE content, which was determined by western blot analysis (Fig. 15). Interestingly, the probe **19** marked different BChE levels in serum samples collected from healthy humans and patients diagnosed with cancer or osteoarthritis (Table 1). The results indicated that the lowest signal recorded was from the breast cancer group, followed by rectal cancer, and the higher signals were detected in the osteoarthritis group, which were followed by the healthy human group (Table 1). **19** monitored the BChE activity in the brain region of female ICR mice. Finally, the probe was employed for the detection of pesticides induced BChE inhibition in HEK293 cells using methomyl, carbofuran and DDVP. The fluorescence signal was considerably reduced in HEK293 cells treated with carbofuran and DDVP. As inhibition efficiency of methomyl on BChE was insignificant, no notable changes in the emission channel were observed in the methomyl treated group. It is not clear why methomyl cannot inhibit BChE activity, thus further investigations are needed.

Table 1 Activity of BChE in different conditions

	Probe	
Condition	**19**	**20**
Healthy	Highest	Highest
Osteoarthritis	High	High
Rectal cancer	Moderate	Low
Breast cancer	Low	Moderate

In 2022, Ding's group followed a four-step synthetic route to prepare an activity-based ratiometric probe (**20**) for BChE detection (Fig. 14).[130] In its caged form, the probe showed an absorption shoulder centered at 416 nm, and a fluorescence maximum at 556 nm. The LOD of **20** was measured as 0.077 μg mL^{-1}. After incubation with BChE (50 μg mL^{-1}) for 40 minutes, a red shift from 416 nm to 616 nm in the absorbance spectrum was observed, which was followed by a hypochromic shift to 486 nm in the emission spectrum. Similar to their probe **19**, the probe **20** was employed for the detection of BChE fluctuations in human serum samples collected from healthy subjects and patients with osteoarthritis, breast cancer and rectal cancer (Table 1). Repeatedly, the highest signals were obtained from the healthy group. Breast cancer and

osteoarthritis samples displayed moderately lower signals than healthy serum samples. As opposed to the previously reported study, the lowest signal was recorded from the rectal cancer group rather than breast cancer (Table 1). The probe also successfully monitored the BChE activity in HEK293 cells and fresh mice brain slices, both in the presence and absence of iso-OMPA.

A flavylium derived and mitochondria targeted BChE responsive probe (**21**) was obtained through a two-step synthetic route by Cao *et al.*, in 2021 (Fig. 14).[131] Introduction of the BChE sensing group blocked the ICT process and thus its fluorescence at 628 nm was quenched. Upon treatment with BChE, the fluorescence intensity of the compound **21** was

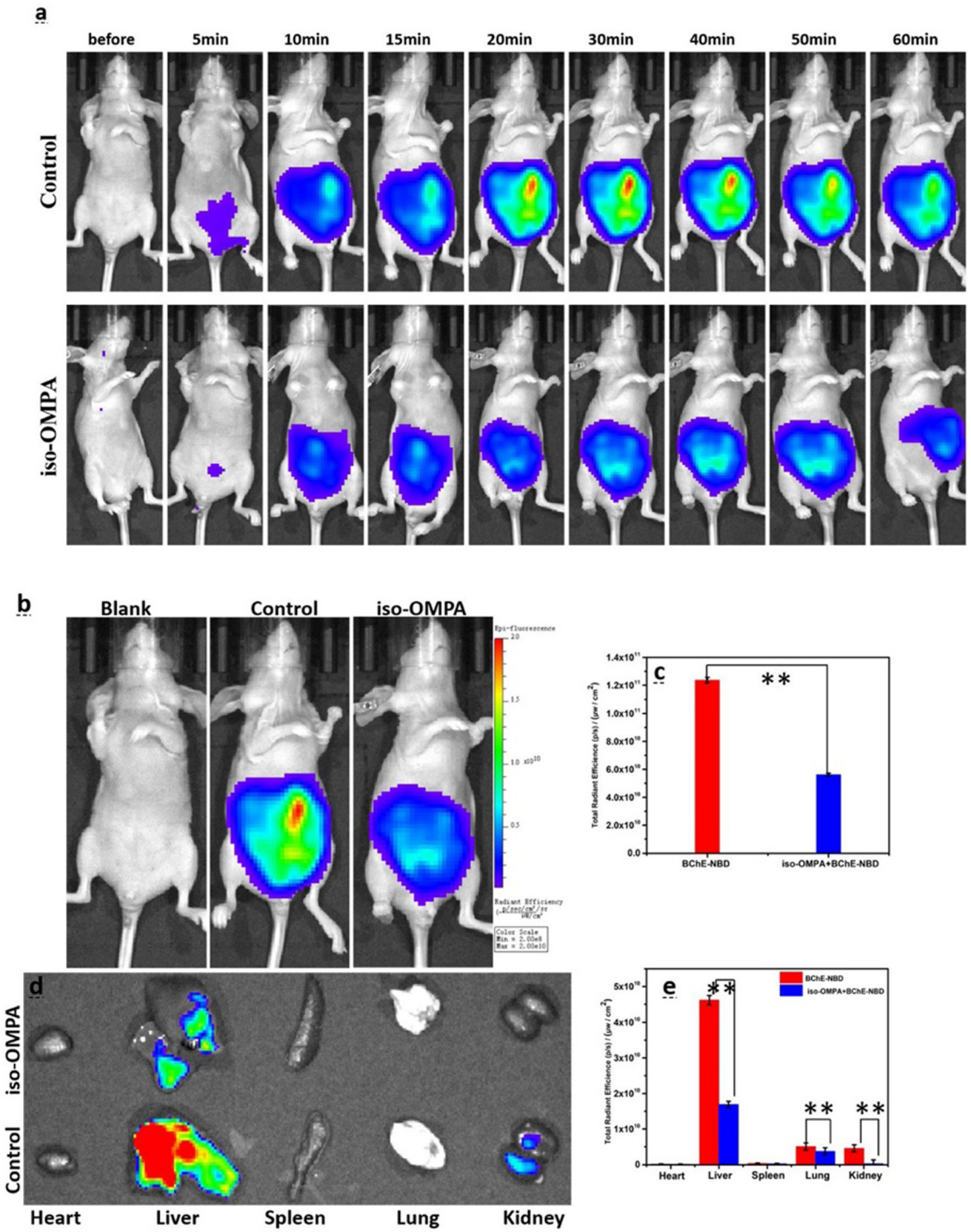

Fig. 16 (a) Time-resolved fluorescence images. (b) Images captured after 30 min. Blank: mice treated with saline; control: mice treated with probe **21**; iso-IMPA: mice treated with iso-OMPA inhibitor and then probe **21**. (c) The emission intensities shown in (b). (d) The fluorescence images of major organs. (e) The emission intensities shown in (d). λ_{ex} = 580 nm, λ_{em} = 600–700 nm. Adapted with permission from ref. 131. Copyright 2021 Elsevier.

gradually increased due to liberation of the emissive NDB core and reached a plateau around 30 minutes. Treatment with tacrine and iso-OMPA inhibited the endogenous BChE, and consequently no signals were detected in HEK293 and HeLa cells. However, no inhibition was observed with the donepezil group due to its specificity toward AChE. The probe was selectively activated by BChE in zebrafish and mice (Fig. 16). The authors demonstrated the BChE distribution in major organs, in which robust signals were detected in the liver, lung, and kidney (Fig. 16).

In 2022, Liu group prepared a set of hemicyanine derived probes (**22–23**) bearing different indole rings to monitor BChE activity (Fig. 17).[132] Compound **22** exhibited a higher fluorescence enhancement (~130 fold) in the presence of BChE, as opposed to **23**, whose response was negligible due to a lower band gap reduction. The fluorescence signal of **22** at 715 nm increased linearly with the addition of increased concentrations of BChE (0–20 ng mL^{-1}), and the LOD was calculated as 0.12 ng mL^{-1}. Compound **22** monitored the endogenous BChE in SH-SY5Y, HepG2 and HEK293 cells. *In vitro* studies indicated that the highest signal was recorded from SH-SY5Y cells, followed by HepG2, and a very low turn ON response was observed from HEK293 cells. Fluorescence recovered from all cells were significantly reduced when the cells were pre-incubated with iso-OMPA.

Impact of forskolin and hydrocortisone on BChE was investigated (Fig. 18) under a confocal microscopy using **22**. In accordance with the recent findings, the fluorescence captured from the red channel was gradually increased upon increasing the concentration of hydrocortisone (0–10 μM), while the signal was dramatically quenched in the forskolin-treated HepG2 cells (Fig. 18). The probe was finally employed for the detection of endogenous BChE in mouse models. Intraperitoneal administration of **22** to healthy mice demonstrated increased fluorescence around the abdominal region, along with an accumulation in the liver according to *ex vivo* studies. A robust fluorescence signal was observed in tumor-bearing mice around the liver tumor region with a 48-fold increase compared to the healthy liver, clearly indicating elevation of BChE levels at the tumor site. Finally, 2- and 6-months old transgenic AD mice (APP/PS1) were treated with **22**, and healthy mice were selected as a control group for comparison. The highest signal was recorded from 6 months old AD-bearing mice, followed by the 2 months old group, and the lowest signal recorded from the control group. This enhanced fluorescence response was also demonstrated through confocal microscopy using brain

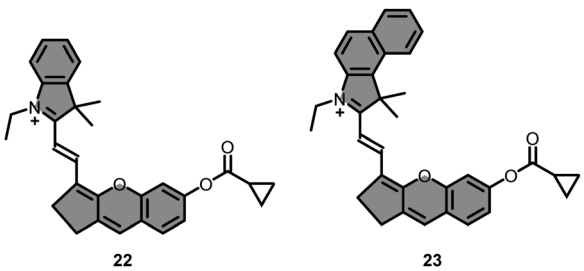

Fig. 17 Molecular structures of compound **22–23**.

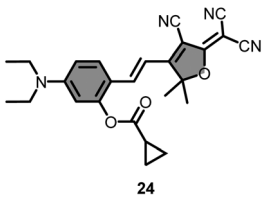

Fig. 19 Molecular structure of compound **24**.

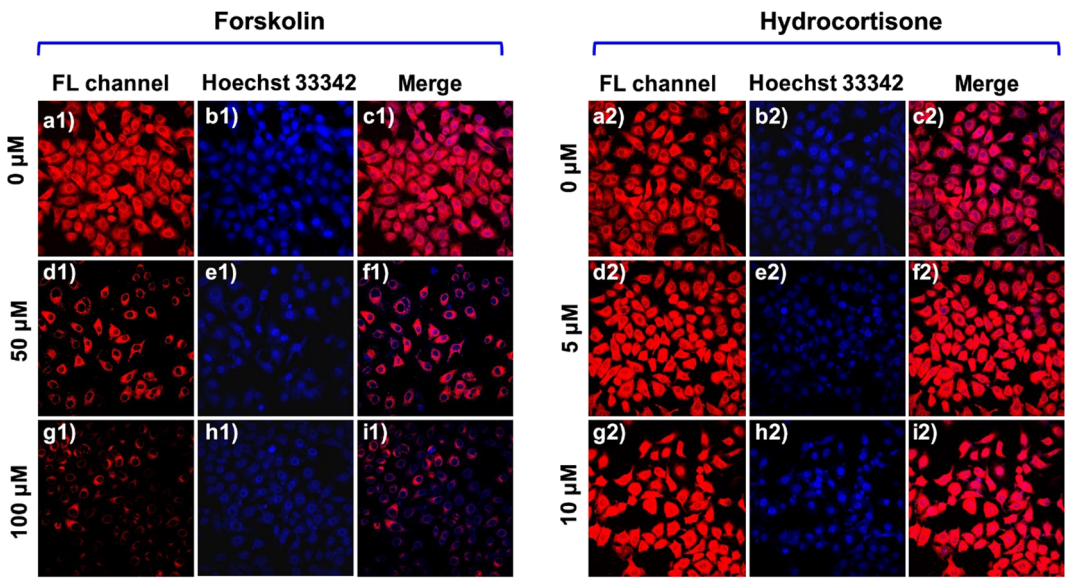

Fig. 18 Fluorescence images of HepG2 cells. Cells treated with only probe **22** (a1–c1 and a2–c2). Cells pre-incubated with different concentrations of foskolin (d1–f1 and g1–i1) or hydrocortisone (d2–f2 and g2–i2) and then treated with probe **22**. Adapted with permission from ref. 132. Copyright 2022 American Chemical Society.

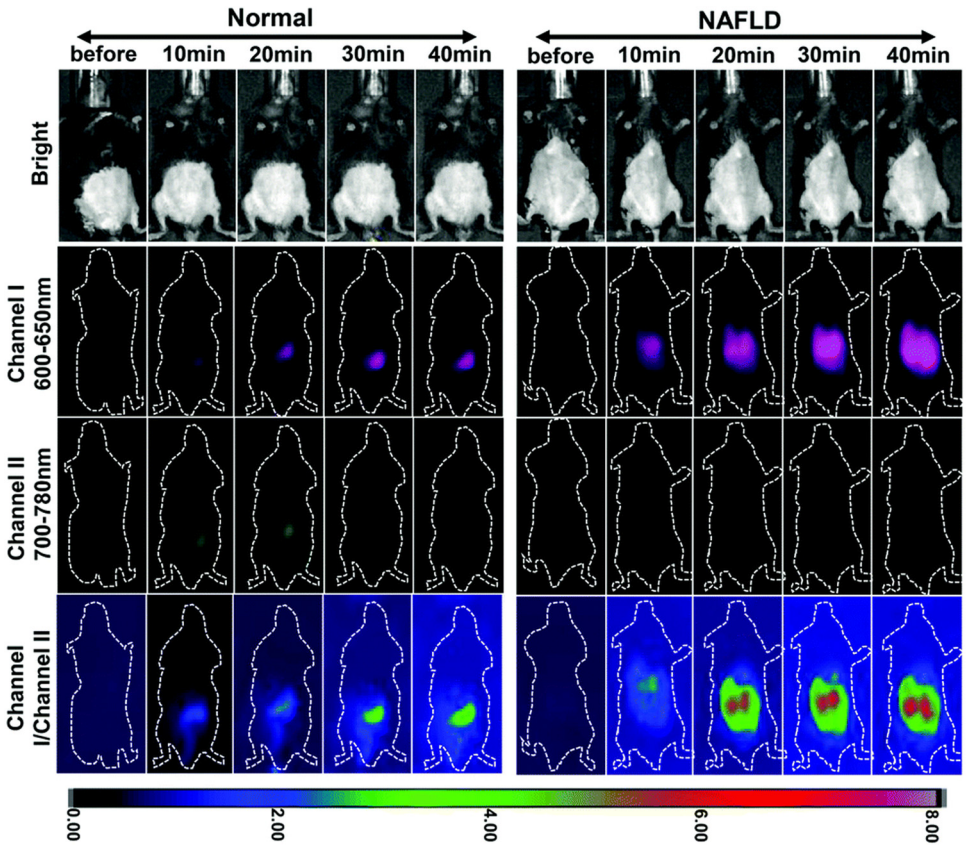

Fig. 20 The ratiometric imaging of normal and NAFLD-bearing mouse models with probe **24** through channel I (600–650 nm), channel II (700–780 nm) and ratio channel (channel I/channel II). Adapted with permission from ref. 133. Copyright 2022 Royal Society of Chemistry.

tissues of the mouse models. Predictably, a similar pattern was observed.

The first example of a BChE-responsive ratiometric AIE probe (**24**) was reported by Xiang *et al.*, in 2022 (Fig. 19).[133] The probe obtained *via* two-step synthesis and manifested a negligible response to AChE. In contrast, introduction of BChE resulted in a slight red shift from 565 nm to 600 nm in the absorbance spectrum while activating the I_{626}/I_{760} ratiometric channel for the detection of BChE. Molecular docking studies of the probe with AChE and BChE revealed that **24** is more suitable for BChE due to its hydrogen bonding and hydrophobic interactions. At the active site, the proximity of Ser198 to the carbonyl group of the sensing unit was 3.18 Å, showing its eligibility for Ser-initiated nucleophilic attack. A 17-fold stronger fluorescence signal at 626 nm was detected 30 minutes after the addition of BChE, while the fold change was 26 in the I_{626}/I_{760} ratiometric channel. The LOD was reported as 39.24 ng mL^{-1}. Compound **24** successfully monitored the BChE activity in HeLa cells and selectively responded to exogenous BChE. The selective activation was further proved under confocal microscopy by treating LO2 cells with different cholinesterase inhibitors. Similar to other probes, no inhibition was observed in donepezil treated cells while a significant drop was observed in tacrine or iso-OMPA treated groups.

Lastly, the probe was injected to normal and nonalcoholic fatty liver disease (NAFLD) bearing mice, and its fluorescence was recorded every 10 minutes for 40 minutes. The fluorescence signal was gradually increased in both groups, but a 3-fold higher signal was detected from the NAFLD group (Fig. 20), which were in good agreement with their serum samples.

Two activity-based probes (**25–26**) with high cell membrane permeability were developed by Liu's group in 2022 (Fig. 21).[134] The LOD of **25** and **26** toward BChE was calculated as 0.12 μg mL^{-1} and 0.13 μg mL^{-1}, respectively. The BChE activity in HepG2 and HEK293 cells were successfully monitored by employing **25** and **26**. Additionally, compound **25** monitored the BChE activity in 5–6 weeks old BALB/c nude mouse models.

An aggregation-induced enhanced emission (AIEE) and excited state intramolecular proton transfer (ESIPT)-based

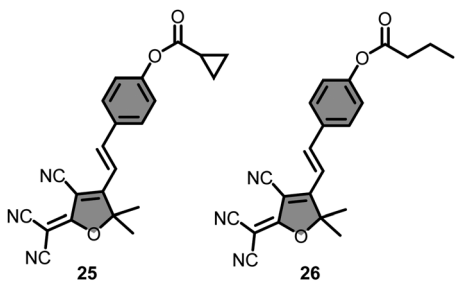

Fig. 21 Molecular structures of compound **25** and **26**.

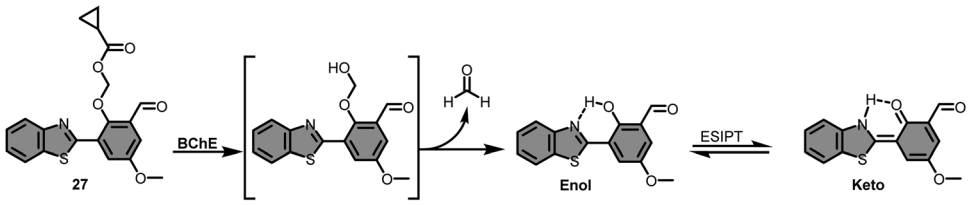

Fig. 22 Molecular structure and activation of compound **27** with BChE.

BChE activatable fluorescent probe (**27**) was obtained through a 3-step synthesis by Pei *et al.*, in 2023.[135] Due to slight changes in the responsive unit, a two-step process was followed during the activation (Fig. 22). The ester bond was cut off by BChE to give an unstable intermediate of an ether derivative, followed by a rapid formaldehyde release, restoring its ESIPT while enhancing fluorescence through keto–enol tautomerization (Fig. 22). Absorption of **27** shifted from 349 nm to 457 nm after treatment with BChE and rendered a large Stokes shift (157 nm) with an LOD of 0.000754 U mL^{-1}. Intracellular BChE in HeLa cells were successfully monitored by **27**. Notably, the findings of Xiang *et al.* were also supported by **27**, as the probe **27** detected a brighter fluorescence emission from the liver of NAFLD zebrafish compared to its normal liver, bearing a similar pattern with **24**.

Taking advantage of the elevated BChE and ROS levels in AD, a series of BChE and ROS targeting methylene blue based probes (**28–30**) were introduced (Fig. 23) by Ding's group, in 2021.[136] Authors aimed for a sequential activation which was initiated by BChE and followed by ROS. Accordingly, the cyclopropyl moiety and phenolic hydroxyl groups were combined, and prolonged with chains of different lengths. Among them, only **29** displayed a dual sensing strategy and did not give any response in the presence or absence of BChE and ROS alone. However, treating **29** with increased concentration of BChE (0–1000 μg mL^{-1}), in the presence of fixed concentration of *t*-$BuOO^-$ (1 mM), steadily recovered its fluorescence at 690 nm upon irradiation at 600 nm. A very high linearity was observed in the range of 0–80 μg mL^{-1}, and the LOD was reported as 1.08 μg mL^{-1}. After satisfactory photophysical characterization, imaging potential of **29** was demonstrated in HEK293 cells. However, only a weak emission was observed in HEK293 cells treated with **29**. As this low emission was attributed to the insufficient expression of endogenous ROS, the cells were treated with PMA. As a result, a very bright image was captured. Furthermore, the selective activation in the cellular environment by BChE and ROSs was also demonstrated by treating the cells with tacrine and *N*-acetylcysteine. Lastly, the accuracy of **29** in detecting AD was assessed by conducting *in vivo* studies. Accordingly, a series of experiments were carried out on 6 months old AD-bearing APP/PS1(B6) and normal C57BL/6j mice. Notably, over 80-fold fluorescence intensity was detected in AD-bearing mice in comparison to the control group. While it is indicative of its potential for early diagnosis of AD, it also supports the current findings on increased levels of BChE and ROS in AD. Additionally, the source of the activation was further investigated by treating APP/PS1(B6) mice with BChE and ROS inhibitors, similar to the *in vitro* studies. In both cases, a significant drop in fluorescence was observed due to the selective inhibition of BChE or ROS in APP/PS1(B6) mice.

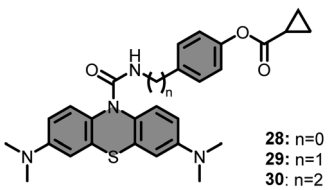

Fig. 23 Molecular structures of compound **28–30**.

In 2023, an ICT-driven BChE selective fluorescent probe (**31**) was developed (Fig. 24) through a three-step synthetic route.[137] The probe not only displayed good photo- and thermostability but also responded to BChE in a linear manner within the concentration range of 0.5–200 U L^{-1}, and its LOD was determined to be 0.056 U L^{-1}. This turn-on response was attributed to a new peak arising on the fluorescence spectrum at 642 nm upon irradiation at 580 nm after introduction of BChE. After evaluating the cytotoxicity, endogenous BChE activity was assessed in cell studies and a weaker signal was detected in HepG2 cells compared to LO2 cells. The fluctuation of BChE was also measured in liver injury models, and lower BChE signals were detected in APAP-induced liver injury groups in both cell and animal studies. As opposed to that, a higher

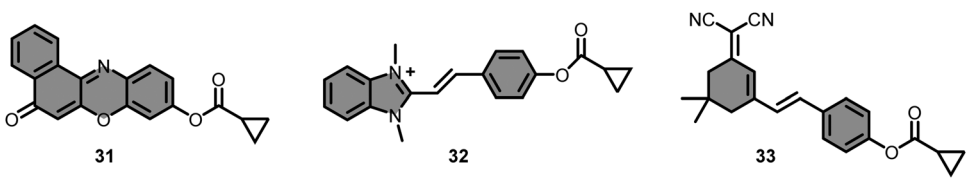

Fig. 24 Molecular structures of compound **31–33**.

turn-on response was detected in diabetic mouse models, which was attributed to the elevated BChE levels.

A cyanine derived BChE responsive fluorescent probe (**32**) with large Stokes shift (113 nm) was obtained (Fig. 24) through a two-step synthetic pathway by Guo *et al.*[138] A red shift from 320 nm to 343 nm was observed on the absorbance spectrum, while its fluorescence was enhanced around 430 nm upon introduction of BChE. The LOD was calculated as 0.07969 U mL^{-1}. Firstly, the probe was utilized to monitor the endogenous BChE in LO2 cells. Then, the probe measured the BChE activity in cells treated with H_2O_2 which were meant to induce apoptosis, and a higher emission signal was recorded from cells treated with H_2O_2.

A photostable and non-toxic fluorescent probe (**33**) was developed (Fig. 24) by Sun *et al.* to monitor BChE activity in thyroid cancer.[139] The probe become emissive at 689 nm upon excitation at 550 nm following the BChE incubation. The probe exhibited a linear turn-on response within the concentration range of 0–900 U L^{-1}, and its LOD was calculated as 3.93 U L^{-1}. This prove evaluated a lower BChE activity in Tpc-1 cells than Nthy-oris-1 normal thyroid cells, following the activity trend between normal and cancer cells.

The emission of light upon a chemical reaction, also known as chemiluminescence, has attracted intense interest in the field of imaging after the development of new generation of phenoxy 1,2-dioxetane based chemiluminescent probes by Shabat group.[140] These probes offer a high signal-to-noise ratio as need for an outer light source is eliminated. Moreover, new generation of chemiluminescent probes have the capability to function under physiological conditions. By leveraging this property, Kolemen group developed a BChE-responsive chemiluminescent probe (**34**) to track BChE activity in live cells and animal models (Fig. 25).[141]

The BChE-induced hydrolysis of the cyclopropyl based masking unit followed by the chemically initiated electron exchange luminescence (CIEEL) mechanism upon formation of phenolate ions, which chemically excited benzoate products were liberated in a consecutive manner to generate chemiluminescence signal (Fig. 25). The LOD of the **34** was calculated as 0.015 U mL^{-1}. The probe successfully evaluated the endogenous BChE activity in HEK293 normal cells in addition to HepG2 liver cancer and SH-SY5Y neuroblastoma cells. Chemiluminescence signal recorded from all cells drastically reduced after tacrine inhibition. The probe selectively monitored the BChE activity in healthy mice in addition to tumor region in SH-SY5Y tumor-bearing mice (Fig. 26).

The molecular sensors responsive to BChE were summarized in Table 2 to provide a clear overview.

Conclusion and future directions

In this review article, we have demonstrated the importance of BChE activity in regard to various human disease states including AD and cancer. Moreover, we have chronologically described the evolution of BChE probes from the advent of first-generation 'always-on' imaging agents to modern activity-based sensing probes capable of reporting on BChE activity in real-time. It is evident that each molecular sensor summarized in this review were prepared elaborately to uncover the unique roles of BChE. However, a few but essential parameters should

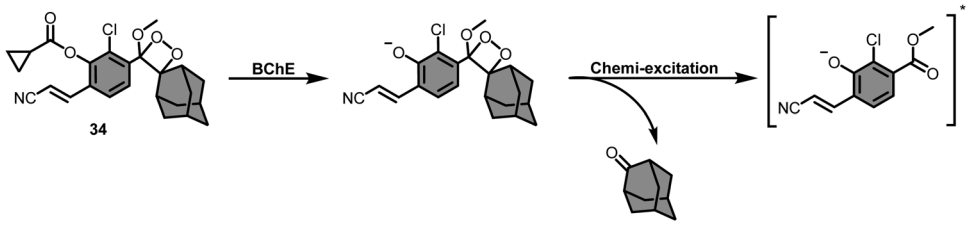

Fig. 25 Molecular structure and activation of compound **34** with BChE.

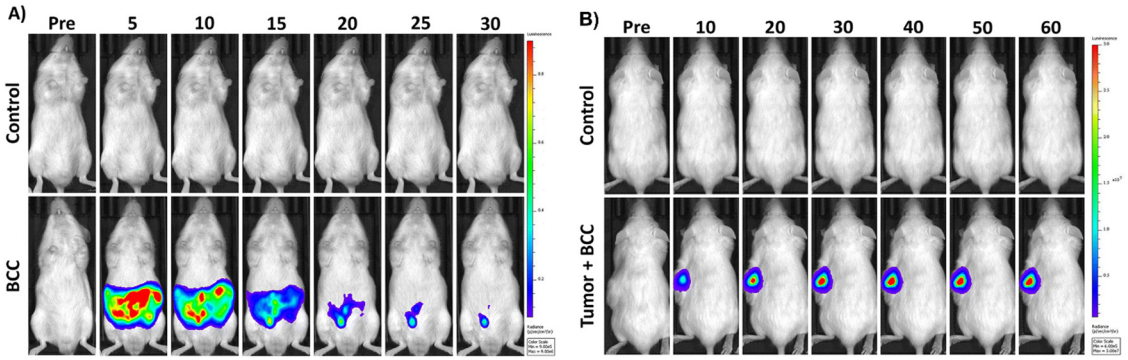

Fig. 26 (A) Time-dependent *in vivo* images of PBS (top) or probe **34** (bottom) treated healthy mice and. (B) Time-dependent *in vivo* images of SH-SY5Y tumor bearing mice. Top row: Subcutaneous injection of PBS. Bottom row: Intratumoral injection of probe **34**. Adapted with permission from ref. 141. Copyright 2023 Royal Society of Chemistry.

Table 2 Summary of BChE responsive molecular sensors

Probe	Type	Mechanism	Abs/Ems (nm)	Limit of detection	Ref.
1a	Fluorophore	Always-on	649/668	n/a	118
1b	Fluorophore	Always-on	650/665	n/a	118
2	Fluorophore	Turn-off	355/520	n/a	119
3	Fluorophore	Turn-on	340/485	0.0012 U mL^{-1}	120
9d	Fluorophore	Turn-on	455/515	n/a	121
12	Fluorophore	Turn-on	665/705	n/a	122
13	Fluorophore	Turn-on	687/708	3.75 U L^{-1}	123
14	Carbon quantum dots		450/523	2.7 U L^{-1}	124
15	Fluorophore	Turn-on	350–400/460	0.06 U L^{-1}	125
16	Fluorophore	Ratiometric	380/460, 570	0.04 U L^{-1}	126
17	Fluorophore	Turn-on	545/654	0.0117 U mL^{-1}	127
18	Fluorophore	Turn-on	555/665	0.08 U mL^{-1}	128
19	Fluorophore	Turn-on	480/528	0.075 μg mL^{-1}	129
20	Fluorophore	Ratiometric	416/486, 556	0.077 μg mL^{-1}	130
21	Fluorophore	Turn-on	580/628	29 ng mL^{-1}	131
22	Fluorophore	Turn-on	670/715	0.12 ng mL^{-1}	132
24	Fluorophore	AIE	600/626	39.24 ng mL^{-1}	133
25	Fluorophore	Turn-on	464/562	0.12 μg mL^{-1}	134
26	Fluorophore	Turn-on	464/562	0.13 μg mL^{-1}	134
27	Fluorophore	ESIPT/AIEE	365/614	0.000754 U mL^{-1}	135
29	Fluorophore	Turn-on	656/690	1.08 μg mL^{-1}	136
31	Fluorophore	Turn-on	580/642	0.056 U L^{-1}	137
32	Fluorophore	Turn-on	343/400–650	0.07969 U mL^{-1}	138
33	Fluorophore	Turn-on	550/689	3.93 U L^{-1}	139
34	Chemiluminescence (1,2-dioxetane)	Turn-on	525[a]	0.0015 U mL^{-1}	141

[a] Chemiluminescence signal at given wavelength.

be noted to obtain more advanced probes for BChE. One major issue is the photostability of the agent, which ensures reliability and accuracy, particularly in continuous monitoring. Another factor is the operating range, which requires fine-tuning depending on the nature of the study. In the case of fluorescent probes, having a large Stokes shift is beneficial to avoid self-absorption, which additionally eliminates the need for filters during animal studies. It is clear that introduction of a bulky substituent minimizes the interference of AChE; however, this calibration should be supported by docking studies. Furthermore, selectivity assays should include carboxylesterases in addition to AChE, as it has been overlooked in numerous studies. Undeniably, important criteria that must be met when developing such probes include achieving selectivity over AChE such that one can confidently attribute probe activation to BChE activity. This has required extensive tuning but excellent results have been demonstrated. Additionally, it is notable that probes exhibiting a large dynamic range, and/or self-calibrating ratiometric readouts have been shown to be indispensable for reliable interpretation of results. As highlighted above, a low LOD is characteristic of many fluorescent probes for BChE. While many of the probes discussed in this review article are suitable for cellular studies, the transition toward longer wavelength emission has enabled the detection of BChE selectivity in various murine models. To compliment these NIR emitting BChE probes, we anticipate several advances will take place to enable deeper tissue imaging. For instance, there has been tremendous interest in further shifting the emission into the NIR-II (also known as SWIR) imaging window as it is believed that the corresponding imaging agents will experience less interference from endogenous pigments such as hemoglobin or oxyhemoglobin. However, one caveat is that a large molecular weight and high hydrophobicity will likely result. On the other hand, photoacoustic imaging, operating in both the NIR and NIR-II range, represents a powerful alternative. Because the corresponding photoacoustic probes are caple of harvesting incident light to yield unperturbed ultrasound signals, it possible to obtain high resolution 3D imaging in deep tissue up to 12 cm. Another option to satisfy deep tissue BChE imaging is to utilize NIR emitting chemiluminescent dioxetanes as these probes offer high signal to noise ratio along with a high sensitivity thanks to lack of external light irradiation. Coupling the aforementioned BChE-responsive triggers to known NIR-II, photoacoustic-active dyes or NIR emitting chemiluminescent probes can open the door for new biological findings.

Conflicts of interest

There are no conflicts to declare.

Acknowledgements

The authors thank Ayça Saymaz for the design of the graphical abstract and Fig. 2, which were created with BioRender.com.

References

1 O. Lockridge, C. F. Bartels, T. A. Vaughan, C. K. Wong, S. E. Norton and L. L. Johnson, *J. Biol. Chem.*, 1987, **262**, 549–557.
2 J. Z. Long and B. F. Cravatt, *Chem. Rev.*, 2011, **111**, 6022–6063.

3 S. Darvesh, D. A. Hopkins and C. Geula, *Nat. Rev. Neurosci.*, 2003, **4**, 131–138.
4 A. Chatonnet and O. Lockridge, *Biochem. J.*, 1989, **260**, 625–634.
5 C. V. Altamirano, C. F. Bartels and O. Lockridge, *J. Neurochem.*, 2000, **74**, 869–877.
6 E. Stedman, E. Stedman and L. H. Easson, *Biochem. J.*, 1932, **26**, 2056–2066.
7 O. Lockridge, *Pharmacol. Ther.*, 1990, **47**, 35–60.
8 M. Gok, C. Cicek and E. Bodur, *J. Neurochem.*, 2023, 1–5.
9 P. Masson, M. T. Froment, P. L. Fortier, J. E. Visicchio, C. F. Bartels and O. Lockridge, *Biochim. Biophys. Acta, Protein Struct. Mol. Enzymol.*, 1998, **1387**, 41–52.
10 J. Massoulié, L. Pezzementi, S. Bon, E. Krejci and F. M. Vallette, *Prog. Neurobiol.*, 1993, **41**, 31–91.
11 C. Mattes, R. Bradley, E. Slaughter and S. Browne, *Life Sci.*, 1996, **58**, 257–261.
12 B. Li, M. Sedlacek, I. Manoharan, R. Boopathy, E. G. Duysen, P. Masson and O. Lockridge, *Biochem. Pharmacol.*, 2005, **70**, 1673–1684.
13 S. M. Nurulain, A. Adem, S. Munir, R. Habib, S. Awan, F. Anwar and S. Batool, *Neurophysiology*, 2020, **52**, 145–158.
14 S. T. George and A. S. Balasubramanian, *Eur. J. Biochem.*, 1981, **121**, 177–186.
15 S. J. Gatley, *Biochem. Pharmacol.*, 1991, **41**, 1249–1254.
16 C. G. Zhan, F. Zheng and D. W. Landry, *J. Am. Chem. Soc.*, 2003, **125**, 2462–2474.
17 D. ØStergaard, J. Viby-Mogensen, H. K. Hanel and L. T. Skovgaard, *Acta Anaesthesiol. Scand.*, 1988, **32**, 266–269.
18 P. Juul, *Clin. Chim. Acta*, 1968, **19**, 205–213.
19 B. N. La Du, C. F. Bartels, C. P. Nogueira, M. Arpagaus and O. Lockridge, *Cell. Mol. Neurobiol.*, 1991, **11**, 79–89.
20 G. Šinko, M. Čalić, A. Bosak and Z. Kovarik, *Anal. Biochem.*, 2007, **370**, 223–227.
21 P. Masson and O. Lockridge, *Arch. Biochem. Biophys.*, 2010, **494**, 107–120.
22 S. Chauhan, S. Chauhan, R. D'Cruz, S. Faruqi, K. K. Singh, S. Varma, M. Singh and V. Karthik, *Environ. Toxicol. Pharmacol.*, 2008, **26**, 113–122.
23 V. Aroniadou-Anderjaska, J. P. Apland, T. H. Figueiredo, M. De Araujo Furtado and M. F. Braga, *Neuropharmacology*, 2020, **181**, 108298.
24 O. Lockridge, *Pharmacol. Ther.*, 2015, **148**, 34–46.
25 C. Zhang, Y. Sun, R. Hu, J. Huang, X. Huang, Y. Li, Y. Yin and Z. Chen, *Sci. Rep.*, 2018, **8**, 4–11.
26 L. Poirier, L. Brun, P. Jacquet, C. Lepolard, N. Armstrong, C. Torre, D. Daudé, E. Ghigo and E. Chabrière, *Sci. Rep.*, 2017, **7**, 19–21.
27 R. D. Richins, I. Kaneva, A. Mulchandani and W. Chen, *Nat. Biotechnol.*, 1997, **15**, 984–987.
28 M. Burnworth, S. J. Rowan and C. Weder, *Chem. – Eur. J.*, 2007, **13**, 7828–7836.
29 L. M. Eubanks, T. J. Dickerson and K. D. Janda, *Chem. Soc. Rev.*, 2007, **36**, 458–470.
30 H. Grigoryan, L. M. Schopfer, C. M. Thompson, A. V. Terry, P. Masson and O. Lockridge, *Chem. – Biol. Interact.*, 2008, **175**, 180–186.
31 A. Fidder, A. G. Hulst, D. Noort, R. de Ruiter, M. J. van der Schans, H. P. Benschop and J. P. Langenberg, *Chem. Res. Toxicol.*, 2002, **15**, 582–590.
32 O. Lockridge and L. M. Schopfer, *Chem. – Biol. Interact.*, 2023, **376**, 110460.
33 G. Amitai, A. Plotnikov, S. Chapman, S. Lazar, R. Gez, D. Loewenthal, K. A. Shurrush, G. Cohen, L. J. Solmesky, H. Barr and A. J. Russell, *Commun. Biol.*, 2021, **4**, 1–8.
34 A. Zandona, M. Katalinić, G. Šinko, A. Radman Kastelic, I. Primožič and Z. Kovarik, *Arch. Toxicol.*, 2020, **94**, 3157–3171.
35 T. Zorbaz, D. Malinak, K. Kuca, K. Musilek and Z. Kovarik, *Chem. – Biol. Interact.*, 2019, **307**, 16–20.
36 J. Zeman, D. Vetchý, A. Franc, S. Pavloková, V. Pitschmann and L. Matějovský, *Eur. J. Pharm. Sci.*, 2017, **109**, 548–555.
37 B. Li, I. Ricordel, L. M. Schopfer, F. Baud, B. Mégarbane, P. Massond and O. Lockridgea, *J. Appl. Toxicol.*, 2010, **30**, 559–565.
38 T. R. Mahoney, S. Luo and M. L. Nonet, *Nat. Protoc.*, 2006, **1**, 1772–1777.
39 C. D. Johnson and R. L. Russell, *J. Neurochem.*, 1983, **41**, 30–46.
40 O. Lockridge, E. G. Duysen and P. Masson, *Anticholinesterase Pesticides: Metabolism, Neurotoxicity, and Epidemiology*, 2011, pp. 25–41.
41 E. G. Duysen, B. Li, S. Darvesh and O. Lockridge, *Toxicology*, 2007, **233**, 60–69.
42 E. G. Duysen, B. Li, W. Xie, L. M. Schopfer, R. S. Anderson, C. A. Broomfield and O. Lockridge, *J. Pharmacol. Exp. Ther.*, 2001, **299**, 528–535.
43 I. Manoharan, R. Boopathy, S. Darvesh and O. Lockridge, *Clin. Chim. Acta*, 2007, **378**, 128–135.
44 O. Cohen-Barak, J. Wildeman, J. Van De Wetering, J. Hettinga, P. Schuilenga-Hut, A. Gross, S. Clark, M. Bassan, Y. Gilgun-Sherki, B. Mendzelevski and O. Spiegelstein, *J. Clin. Pharmacol.*, 2015, **55**, 573–583.
45 National Library of Medicine, **https://clinicaltrials.gov/study/NCT00333515** (accessed October 2023).
46 National Library of Medicine, **https://clinicaltrials.gov/study/NCT00333528** (accessed October 2023).
47 Y. Ashani, S. Shapira, D. Levy, A. D. Wolfe, B. P. Doctor and L. Raveh, *Biochem. Pharmacol.*, 1991, **41**, 37–41.
48 N. Allon, L. Raveh, E. Gilat, E. Cohen, J. Grunwald and Y. Ashani, *Toxicol. Sci.*, 1998, **43**, 121–128.
49 B. P. Doctor and A. Saxena, *Chem. – Biol. Interact.*, 2005, **157–158**, 167–171.
50 P. Masson and F. Nachon, *J. Neurochem.*, 2017, **142**, 26–40.
51 P. Zhang, P. Jain, C. Tsao, A. Sinclair, F. Sun, H. C. Hung, T. Bai, K. Wu and S. Jiang, *J. Controlled Release*, 2016, **230**, 73–78.
52 L. M. Schopfer, E. David, S. H. Hinrichs and O. Lockridge, *PLoS One*, 2023, **18**, 1–20.

53 O. Lockridge, L. M. Schopfer, G. Winger and J. H. Woods, *J. Med. Chem. Biol. Radiol. Def.*, 2005, **3**, nihms5095.
54 X. Brazzolotto, M. Wandhammer, C. Ronco, M. Trovaslet, L. Jean, O. Lockridge, P. Y. Renard and F. Nachon, *FEBS J.*, 2012, **279**, 2905–2916.
55 O. Lockridge, E. David, L. M. Schopfer, P. Masson, X. Brazzolotto and F. Nachon, *J. Chromatogr. B: Anal. Technol. Biomed. Life Sci.*, 2018, **1102–1103**, 109–115.
56 M. Bonichon, V. Valbi, A. Combès, C. Desoubries, A. Bossée and V. Pichon, *Anal. Bioanal. Chem.*, 2018, **410**, 1039–1051.
57 H. Mehrani, *Process Biochem.*, 2004, **39**, 877–882.
58 K. Mrvova, L. Obzerova, E. Girard, E. Krejci and A. Hrabovska, *Chem. – Biol. Interact.*, 2013, **203**, 348–353.
59 S. Treskatis, C. Ebert and P. G. Layer, *J. Neurochem.*, 1992, **58**, 2236–2247.
60 L. M. Schopfer, P. Masson, P. Lamourette, S. Simon and O. Lockridge, *Anal. Biochem.*, 2014, **461**, 17–26.
61 J. L. S. Sporty, S. W. Lemire, E. M. Jakubowski, J. A. Renner, R. A. Evans, R. F. Williams, J. G. Schmidt, M. J. V. Der Schans, D. Noort and R. C. Johnson, *Anal. Chem.*, 2010, **82**, 6593–6600.
62 R. S. Naik, T. Belinskaya, C. R. Vinayaka and A. Saxena, *Chem. – Biol. Interact.*, 2020, **330**, 109225.
63 C. R. Crane, D. C. Sanders and J. K. Abbot, *Studies on the storage stability of human blood cholinesterases: I*, U.S. Department of Transportation, Federal Aviation Administration, Office of Aviation Medicine, 1970.
64 A. Saxena, W. Sun, C. Luo and B. P. Doctor, *Chem. – Biol. Interact.*, 2005, **157–158**, 199–203.
65 B. P. Doctor, A. Saxena, W. Sun, C. Luo, P. Tipparaju, I. Koplovitz, D. E. Lenz and M. C. Ross, *US Pat.*, 2006/0194301A1, 2006.
66 C. Silva, M. Martins, S. Jing, J. Fu and A. Cavaco-Paulo, *Crit. Rev. Biotechnol.*, 2018, **38**, 335–350.
67 N. Garti, *Colloids Surf., A*, 1999, **152**, 125–146.
68 A. Arsiccio and R. Pisano, *J. Pharm. Sci.*, 2020, **109**, 2116–2130.
69 D. J. McClements, *Curr. Opin. Colloid Interface Sci.*, 2004, **9**, 305–313.
70 S. A. Braham, E. H. Siar, S. Arana-Peña, H. Bavandi, D. Carballares, R. Morellon-Sterling, D. de Andrades, J. F. Kornecki and R. Fernandez-Lafuente, *Process Biochem.*, 2021, **102**, 108–121.
71 A. L. Fink, *Cryobiology*, 1986, **23**, 28–37.
72 M. Pazhang, N. Mardi, F. Mehrnejad and N. Chaparzadeh, *Int. J. Biol. Macromol.*, 2018, **108**, 1339–1347.
73 P. K. Das and J. Liddell, *Biochem. J.*, 1970, **116**, 875–881.
74 J. S. Ralston, A. R. Main, B. F. Kilpatrick and A. L. Chasson, *Biochem. J.*, 1983, **211**, 243–250.
75 J. Grunwald, D. Marcus, Y. Papier, L. Raveh, Z. Pittel and Y. Ashani, *J. Biochem. Biophys. Methods*, 1997, **34**, 123–135.
76 H. Muensch, H. Goedde and A. Yoshida, *Eur. J. Biochem.*, 1976, **70**, 217–223.
77 Y. Nicolet, O. Lockridge, P. Masson, J. C. Fontecilla-Camps and F. Nachon, *J. Biol. Chem.*, 2003, **278**, 41141–41147.
78 D. Suárez and M. J. Field, *Proteins: Struct., Funct., Bioinf.*, 2005, **59**, 104–117.
79 L. Fang, Y. Pan, J. L. Muzyka and C. G. Zhan, *J. Phys. Chem. B*, 2011, **115**, 8797–8805.
80 W. Hodgkin, E. R. Giblett, H. Levine, W. Bauer and A. G. Motulsky, *J. Clin. Invest.*, 1965, **44**, 486–493.
81 S. Xing, Q. Li, B. Xiong, Y. Chen, F. Feng, W. Liu and H. Sun, *Med. Res. Rev.*, 2021, **41**, 858–901.
82 L. Santarpia, I. Grandone, F. Contaldo and F. Pasanisi, *J. Cachexia Sarcopenia Muscle*, 2013, **4**, 31–39.
83 Y. Gu, M. J. Chow, A. Kapoor, W. Mei, Y. Jiang, J. Yan, J. De Melo, M. Seliman, H. Yang, J. C. Cutz, M. Bonert, P. Major and D. Tang, *Transl. Oncol.*, 2018, **11**, 1012–1022.
84 M. D. Stojanov, D. M. Jovičić, S. P. Djurić, M. M. Konjević, Z. M. Todorović and M. Š. Prostran, *Clin. Biochem.*, 2009, **42**, 22–26.
85 S. Lurie, O. Sadan, G. Oron, A. Fux, M. Boaz, T. Ezri, A. Golan and J. Bar, *Reprod. Sci.*, 2007, **14**, 192–196.
86 S. Onder, L. M. Schopfer, W. Jiang, O. Tacal and O. Lockridge, *Neurotoxicology*, 2022, **90**, 1–9.
87 K. M. Mattila, J. O. Rinne, M. Roytta, P. Laippala, T. Pietila, H. Kalimo, T. Koivula, H. Frey and T. Lehtimaki, *J. Med. Genet.*, 2000, **37**, 766–770.
88 J. Sirviö, H. S. Soininen, R. Kutvonen, J. M. Hyttinen, E. L. Helkala and P. J. Riekkinen, *J. Neurol. Sci.*, 1987, **81**, 273–279.
89 Q. Li, H. Yang, Y. Chen and H. Sun, *Eur. J. Med. Chem.*, 2017, **132**, 294–309.
90 S. Awan, A. N. Hashmi, R. Taj, S. Munir, R. Habib, S. Batool, M. Azam, R. Qamar and S. M. Nurulain, *Biochem. Genet.*, 2022, **60**, 720–737.
91 G. Inácio Lunkes, F. Stefanello, D. Sausen Lunkes, V. Maria Morsch, M. R. C. Schetinger and J. F. Gonçalves, *Diabetes Res. Clin. Pract.*, 2006, **72**, 28–32.
92 M. X. Dong, X. M. Xu, L. Hu, Y. Liu, Y. J. Huang and Y. D. Wei, *BioMed Res. Int.*, 2017, 1524107.
93 S. Awan, A. N. Hashmi, R. Taj, S. Munir, R. Habib, S. Batool, M. Azam, R. Qamar and S. M. Nurulain, *Biochem. Genet.*, 2022, **60**, 720–737.
94 E. K. Perry, R. H. Perry, G. Blessed and B. E. Tomlinson, *Neuropathol. Appl. Neurobiol.*, 1978, **4**, 273–277.
95 S. Darvesh, G. A. Reid and E. Martin, *Curr. Alzheimer Res.*, 2010, **999**, 1–15.
96 T. Sato, Y. Nakamura, Y. Shiimura, H. Ohgusu, K. Kangawa and M. Kojima, *J. Biochem.*, 2012, **151**, 119–128.
97 V. P. Chen, Y. Gao, L. Geng and S. Brimijoin, *Int. J. Obes.*, 2017, **41**, 1413–1419.
98 T. D. Müller, R. Nogueiras, M. L. Andermann, Z. B. Andrews, S. D. Anker, J. Argente, R. L. Batterham, S. C. Benoit, C. Y. Bowers, F. Broglio, F. F. Casanueva, D. D'Alessio, I. Depoortere, A. Geliebter, E. Ghigo, P. A. Cole, M. Cowley, D. E. Cummings, A. Dagher, S. Diano, S. L. Dickson, C. Diéguez, R. Granata, H. J. Grill, K. Grove, K. M. Habegger, K. Heppner, M. L. Heiman, L. Holsen, B. Holst, A. Inui, J. O. Jansson, H. Kirchner, M. Korbonits, B. Laferrère, C. W. LeRoux, M. Lopez, S. Morin,

M. Nakazato, R. Nass, D. Perez-Tilve, P. T. Pfluger, T. W. Schwartz, R. J. Seeley, M. Sleeman, Y. Sun, L. Sussel, J. Tong, M. O. Thorner, A. J. van der Lely, L. H. T. van der Ploeg, J. M. Zigman, M. Kojima, K. Kangawa, R. G. Smith, T. Horvath and M. H. Tschöp, *Mol. Metab.*, 2015, **4**, 437–460.

99 S. Brimijoin, V. P. Chen, Y. P. Pang, L. Geng and Y. Gao, *Chem. – Biol. Interact.*, 2016, **259**, 271–275.

100 B. Li, E. G. Duysen and O. Lockridge, *Chem. – Biol. Interact.*, 2008, **175**, 88–91.

101 L. M. Schopfer, O. Lockridge and S. Brimijoin, *Gen. Comp. Endocrinol.*, 2015, **224**, 61–68.

102 V. P. Chen, Y. Gao, L. Geng, R. J. Parks, Y. P. Pang and S. Brimijoin, *Proc. Natl. Acad. Sci. U. S. A.*, 2015, **112**, 2251–2256.

103 D. Dingova, J. Leroy, A. Check, V. Garaj, E. Krejci and A. Hrabovska, *Anal. Biochem.*, 2014, **462**, 67–75.

104 Y. Zhang, Y. Cai, Z. Qi, L. Lu and Y. Qian, *Anal. Chem.*, 2013, **85**, 8455–8461.

105 M. Zhang, C. Wang, Y. Wang, F. Li and D. Zhu, *J. Mater. Chem. B*, 2023, **11**, 4014–4019.

106 M. Pohanka, *Int. J. Electrochem. Sci.*, 2016, **11**, 7440–7452.

107 A. D. Khattab, C. H. Walker, G. Johnston, M. K. Siddiqui and P. W. Saphier, *Environ. Toxicol. Chem.*, 1994, **13**, 1661–1667.

108 J. Chan, S. C. Dodani and C. J. Chang, *Nat. Chem.*, 2012, **4**, 973–984.

109 S. Erbas-Cakmak, S. Kolemen, A. C. Sedgwick, T. Gunnlaugsson, T. D. James, J. Yoon and E. U. Akkaya, *Chem. Soc. Rev.*, 2018, **47**, 2228–2248.

110 X. Wu, J. M. An, J. Shang, E. Huh, S. Qi, E. Lee, H. Li, G. Kim, H. Ma, M. S. Oh, D. Kim and J. Yoon, *Chem. Sci.*, 2020, **11**, 11285–11292.

111 J. J. Wang and E. H. Cao, *Clin. Chim. Acta*, 2004, **347**, 103–109.

112 X. Wu, W. Shi, X. Li and H. Ma, *Angew. Chem., Int. Ed.*, 2017, **56**, 15319–15323.

113 L. Lan, X. Ren, J. Yang, D. Liu and C. Zhang, *Bioorg. Chem.*, 2020, **94**, 103388.

114 A. Singh, M. Gao and M. W. Beck, *RSC Med. Chem.*, 2021, **12**, 1142–1153.

115 A. C. Sedgwick, L. Wu, H. H. Han, S. D. Bull, X. P. He, T. D. James, J. L. Sessler, B. Z. Tang, H. Tian and J. Yoon, *Chem. Soc. Rev.*, 2018, **47**, 8842–8880.

116 H. Li, Y. Kim, H. Jung, J. Y. Hyun and I. Shin, *Chem. Soc. Rev.*, 2022, **51**, 8957–9008.

117 J. M. An, K. O. Jung, M. S. Oh and D. Kim, *Dyes Pigm.*, 2023, **215**, 111267.

118 S. Chao, E. Krejci, V. Bernard, J. Leroy, L. Jean and P. Y. Renard, *Chem. Commun.*, 2016, **52**, 11599–11602.

119 S. Kang, S. Lee, W. Yang, J. Seo and M. S. Han, *Org. Biomol. Chem.*, 2016, **14**, 8815–8820.

120 S. Yoo and M. S. Han, *Chem. Commun.*, 2019, **55**, 14574–14577.

121 S. H. Yang, Q. Sun, H. Xiong, S. Y. Liu, B. Moosavi, W. C. Yang and G. F. Yang, *Chem. Commun.*, 2017, **53**, 3952–3955.

122 S. Y. Liu, H. Xiong, J. Q. Yang, S. H. Yang, Y. Li, W. C. Yang and G. F. Yang, *ACS Sens.*, 2018, **3**, 2118–2128.

123 J. Ma, X. Lu, H. Zhai, Q. Li, L. Qiao and Y. Guo, *Talanta*, 2020, **219**, 121278.

124 G. Chen, H. Feng, X. Jiang, J. Xu, S. Pan and Z. Qian, *Anal. Chem.*, 2018, **90**, 1643–1651.

125 G. Chen, H. Feng, W. Xi, J. Xu, S. Pan and Z. Qian, *Analyst*, 2019, **144**, 559–566.

126 X. Xu, Y. Cen, G. Xu, F. Wei, M. Shi and Q. Hu, *Biosens. Bioelectron.*, 2019, **131**, 232–236.

127 Y. Ma, W. Gao, S. Ma, Y. Liu and W. Lin, *Anal. Chem.*, 2020, **92**, 13405–13410.

128 W. da Zhang, J. M. Zhang, C. Z. Qin, X. R. Wang and Y. B. Zhou, *Anal. Chim. Acta*, 2022, **1235**, 340540.

129 Q. Zhang, C. Fu, X. Guo, J. Gao, P. Zhang and C. Ding, *ACS Sens.*, 2021, **6**, 1138–1146.

130 C. Wan, J. Li, J. Gao, H. Liu, Q. Zhang, P. Zhang and C. Ding, *Dyes Pigm.*, 2022, **197**, 109874.

131 T. Cao, L. Zheng, L. Zhang, Z. Teng, J. Qian, H. Ma, J. Wang, Y. Cao, W. Qin and Y. Liu, *Sens. Actuators, B*, 2021, **330**, 129348.

132 Y. Yang, L. Zhang, J. Wang, Y. Cao, S. Li, W. Qin and Y. Liu, *Anal. Chem.*, 2022, **94**, 13498–13506.

133 C. Xiang, J. Xiang, X. Yang, C. Li, L. Zhou, D. Jiang, Y. Peng, Z. Xu, G. Deng, B. Zhu, P. Zhang, L. Cai and P. Gong, *J. Mater. Chem. B*, 2022, **10**, 4254–4260.

134 Y. Yang, L. Zhang, J. Wang, Y. Cao, W. Qin and Y. Liu, *Dyes Pigm.*, 2022, **206**, 110596.

135 X. Pei, Y. H. Fang, H. Gu, S. Zheng, X. Bin, F. Wang, M. He, S. Lu and X. Chen, *Spectrochim. Acta, Part A*, 2023, **287**, 122044.

136 P. Zhang, C. Fu, H. Liu, X. Guo, Q. Zhang, J. Gao, W. Chen, W. Yuan and C. Ding, *Anal. Chem.*, 2021, **93**, 11337–11345.

137 L. Xu, M. Ma, J. Li, H. Yang, D. Gao, P. Ma and D. Song, *Sens. Actuators, B*, 2023, **394**, 134432.

138 Z. Yu, X. Li, X. Lu and Y. Guo, *New J. Chem.*, 2022, **46**, 12034–12040.

139 W. Kang, M. Ma, L. Xu, S. Tang, J. Li, P. Ma, D. Song and Y. Sun, *Anal. Chim. Acta*, 2023, **1282**, 0–7.

140 O. Green, T. Eilon, N. Hananya, S. Gutkin, C. R. Bauer and D. Shabat, *ACS Cent. Sci.*, 2017, **3**, 349–358.

141 A. Acari, T. Almammadov, M. Dirak, G. Gulsoy and S. Kolemen, *J. Mater. Chem. B*, 2023, **11**, 6881–6888.